Article

Fluid inclusion studies of barite disseminated in hydrothermal sediments of the Mohns Ridge

Marina D. Kravchishina * , Vsevolod Yu. Prokofief , Olga M. Dara , Boris V. Baranov , Alexey A. Klyuvitkin , Karina S. Iakimova , Vladislav Yu. Kalgin , Alla Yu. Lein

Posted Date: 7 July 2023

doi: 10.20944/preprints202307.0468.v1

Keywords: barite; fluid inclusion; hydrothermal vent field; hydrothermal fluid; mineralization; volcanogenic massive sulfide deposits; ultraslow-spreading ridge; Mohns Ridge; Arctic Mid-Ocean Ridge.

Article

Fluid Inclusion Studies of Barite Disseminated in Hydrothermal Sediments of the Mohns Ridge

Marina D. Kravchishina [1]*, Vsevolod Yu. Prokofief [2], Olga M. Dara [1], Boris V. Baranov [1], Alexey A. Klyuvitkin [1], Karina S. Iakimova [1,3], Vladislav Yu. Kalgin [1] and Alla Yu. Lein [1]

[1] Shirshov Institute of Oceanology, Russian Academy of Sciences, 36 Nakhimovsky Prosp., Moscow 117997, Russia; kravchishina@ocean.ru (M.D.K.); olgadara@mail.ru (O.MD.); bbaranov@ocean.ru (B.V.B.); klyuvitkin@ocean.ru (A.A.K.); yakikarina@gmail.com (K.S.Ya.); kalgin.vladislav@yandex.ru (V.Yu.K.); allaulein@gmail.com (A.Yu.L.)
[2] Institute of Geology of Ore Deposits, Petrography, Mineralogy, and Geochemistry, Russian Academy of Sciences, 35 Staromonetny Per., Moscow 119017, Russia; vpr2004@rambler.ru (V.Yu.P.)
[3] Lomonosov Moscow State University, GSP-1, Leninskie Gory, Moscow, 119991, Russia; yakikarina@gmail.com (K.Ya.)
* Correspondence: kravchishina@ocean.ru; Tel.: +7 499 1247737

Abstract: This article discusses the results of fluid inclusions study in barite collected at the Jan Mayen vent field area (Troll Wall and Perle & Bruce) and Loki's Castle vent field of the Mohns Ridge segment of the Arctic Mid-Ocean Ridge. Three mafic-hosted volcanogenic massive sulfide deposits were examined within the active vent fields that adequately correspond to geological settings of ultraslow-spreading ridges and *PT*-conditions. Hydrothermal sediments were investigated to determine the temperature and salinity of the fluids responsible for barite precipitation. The hydrothermal origin of the barite was confirmed by its morphology. Fluid inclusions are two-phase and homogenized into the liquid phase on heating at temperatures below 287ºC. The *salt concentration* in *fluids* trapped in inclusions is 2.6–4.4 wt.% NaCl eq. The crystallization temperatures varied from 276ºC to 119ºC and from 307ºC to 223ºC for the Jan Mayen and Loki's Castle vent fields, respectively. The data obtained allowed us to confirm evidence of fluid phase separation in the hydrothermal systems and to expand our knowledge of the temperature and salinity of mineral fluids previously known from recent direct measurements during the cruises within the G.O. Sars research vessel. The fluid inclusions data obtained from barites emphasize the fluid features characteristic of volcanogenic massive sulfide deposits, the similarities and differences for the studied hydrothermal sites, and allow comparisons with similar products from other active hydrothermal systems.

Keywords: barite; fluid inclusion; hydrothermal vent field; *hydrothermal* fluid; mineralization; volcanogenic massive sulfide deposits; *ultraslow-spreading ridge; Mohns Ridge;* Arctic Mid-Ocean Ridge

1. Introduction

The major dissolved–particulate transformation of Ba in the ocean is related to the mineral $BaSO_4$ (barite). Barite, a mineral of the natural sulfate class often containing the Sr admixture, is characterized by the orthorhombic syngony. Barite is one of the most abundant authigenic minerals in deep ocean sediments [1] and one of the few authigenic minerals that may form in the water column during the microbial oxidation of sinking organic matter (e.g., [2,3]). Two main genetic types of barite form in the marine realm: (i) sedimentary barite – particulate crystals formed usually due to "passive" biogeochemical precipitation in seawater (pelagic barite) and more rarely – through "active" biological pathway by several planktonic organisms (biogenic barite) [4]; (ii) diagenetic or fluid-related barite formed via diagenetic processes with participation of pore water of sediments or reduced fluids of cold seeps and hydrothermal vents [5,1,6]. The diagenetic type, *in our view,* includes barites formed from the reduced solutions during their mixing with the oxidized ocean water. Such solutions are divided into the pore waters in sediments, gas–water solutions in methane seeps, and hydrothermal solutions in mid-ocean rift valleys.

The size and morphology of barite crystals formed by those different precipitation pathways are distinct [5]. The formation of pelagic barite is closely linked to the formation of particulate organic-rich aggregates in the mesopelagic zone of the ocean and heterotrophic remineralization of organic matter in particle-associated microenvironments [3,7]. The micro-crystals of pelagic barite from 200 nm to 2 μm are ubiquitous in the ocean and are typically ellipsoidal in shape [7,4]. Diagenetic barite may form at the water–sediment interface or below the seafloor from reduced pore water of sediments when mixed with oxidized seawater-hosted SO_4^{2-} [e.g., 8]. The similar pathway led to the formation of cold seep and hydrothermal barite, therefore different Ba-rich fluids are discharged through seeps or ridge systems into sulfate-rich seawater, and barite saturation is exceeded [9,10]. Diagenetic barite crystals are large (20–700 μm), flat, tabular-shaped crystals and appear as barite beds in the sedimentary column [5]. Hydrothermal barite is formed by the discharge of modified seawater-derived hydrothermal fluids heated by underlying magmas. Recent studies [11,12,13] indicated that barite in hydrothermal systems did not necessarily precipitate from a mixture of ambient seawater and a hydrothermal fluid and microbial sulfate reduction is also taking place in hydrothermal environments. Hydrothermal barite crystals are also larger (~10–700 μm) and are typically precipitated as cross cutting tabular crystals commonly forming rosettes (roses, druses, brooms, and others) [5,6]. One can also see barite intergrowths as compact platy and granular aggregates and zoned nodules. Hydrothermal barite precipitates from mantle derived fluids influenced by hydrothermal processes. Ba is leached from the oceanic crust (basalt), and when the circulating fluids interact and mix with sulfate-rich seawater, barite may precipitate. The S isotope ratio of hydrothermal barite is usually a mixture of present-day seawater S and hydrothermal origin S (H_2S oxidation) [e.g., 5]. It is well known [e.g., 14], that Sr is a common trace substitution in barite structure. Hydrothermal barite is characterized by the Sr isotope ($^{87}Sr/^{86}Sr$) ratio often occupying an intermediate position between the modern value in seawater and the isotopic composition in pure hydrothermal fluids [15]. Anyway, the precipitation of barite at the hydrothermal vent fields is confined to the redox barrier and related to the formation mechanism similar to that of the diagenetic pathway [6].

Barite is allegedly characterized by short-range migration. Seawater as a rule is a Ba-unsaturated environment [16]. The barite dissolution rates in seawater, as that of sphalerite (often paragenetically associated with barite) and anhydrite depends on the size of crystals, but it is generally extremely lower than, for example, the solubility of carbonates [1]. Barite behaves as a closed system under typical oxic seafloor conditions, and is not prone to diagenetic alteration [e.g., 14]. Hydrothermal barite occurs in the ocean mainly in the low- and medium-temperature hydrothermal sediments, chimneys, nodules, and metalliferous sediments [17,18]. Barium concentration in the primary (end member) hot solutions of hydrothermal vent fields in the Mid-Atlantic Ridge (MAR) and East Pacific Rise (EPR) differ ~20 times depending on the depth and solution temperature, as well as the composition of initial igneous rocks (felsic rocks, basalts, or ultramafic rocks) and can reach 789 μM [19]. Some part of Ba enters the plume in the water column, while ~5% of hydrothermal Ba flux precipitates together with sulfides and nonmetallic minerals in the composition of edifices, sometimes as barite chimneys like in the Loki's Castle vent field, Mohns Ridge [13]. The recent constraints on hydrothermal Ba compositions [20] enable the hydrothermal input of Ba to Atlantic deep waters to be assessed at 3–9% of the observed Ba.

Hydrothermal vent fields in the ocean are divided into several varieties depending on their location relative to the rift system (rifts in the mid-ocean ridge, back-arc spreading, and intraplate volcanism zones), as well as on the ocean depth and, hence, on *PT*-conditions and composition of the initial igneous, felsic to ultramafic, rocks [19]. In addition to black smokers, gray and white smokers are also identified in the ocean. Temperature of hydrothermal solutions in black smokers varies from 185 to 363°C. Such temperatures are unfavorable for the barite formation. Low and medium temperatures (~20–200°C) and ocean depth of about 1500 m are most favorable for the hydrothermal barite precipitation [13,18,21,22,23,24,25].

Fluids are trapped as fluid inclusions in some minerals formed during the hydrothermal process [26,27]. Fluid inclusions (FIs) in minerals are studied to establish parameters of the often inaccessible primary hydrothermal solution [26–29]. FIs are fluid-filled vacuoles sealed within minerals. Based on the gas–liquid (i.e., fluid) inclusions in barite crystals, as in anhydrite and calcite crystals, ones can determine the pressure, temperature and salinity of primary solutions. Barite crystals may represent a combination of two formation processes involving hot fluids and pore water in the sediment covered ridge system that interact and mix with sulfate-rich seawater [5,13,30]. Samples of barite collected in the Guaymas Basin provide such an example where the fluids are expelled into marine-sediment strata where sulfate reduction takes place, depleting the pore-water sulfate from the light S isotope and resulting in barite with S isotope ratios slightly greater than seawater [30]. In this regard, when studying FIs in barites, each time the question should arise about the *feasibility* of using them for determination of temperature and salinity of pure (mantle derived) hydrothermal fluids. There are a number of problems that are frequently encountered in the study of FIs and many of these problems are critical for the validity of the FIs data and their interpretations [31, and the references therein]. Nevertheless barite crystals preserve geochemical fingerprints associated with conditions of formation and are especially important as a key structural component to hydrothermal edifices on the seafloor [17,18].

The high preservation potential of barite and its resistance to diagenetic alteration after burial in oxic settings make this authigenic mineral favourable for studies of the origin of formation fluids [1]. Barite has no a retrograde solubility unlike relatively fast-soluble anhydrite, persisting in hydrothermal structures longer than anhydrite. On the Mohns Ridge, several successful attempts have been made to directly measure the temperature of hydrothermal fluids [i.e., 32,33,34]. However, these measurements are challenging and require confirmation by other methods. Another reliable approach is fluid inclusion microthermometry in hydrothermal minerals, in barites *particularly [27,35,36].* Previous studies [37] investigated the FIs in anhydrite within the Fåvne hydrothermal vent field recently discovered at the Mohns Ridge. There are no reports of FIs hosted in barite within the hydrothermal vent fields studied along the Mohns Ridge [38,39]. To address the lack of published information on the hydrothermal FIs we performed microthermometric measurements of fluid inclusions hosted in barite within the mineral assemblages of the active Troll Wall, Perle & Bruse and Loki's Castle vent fields. Our data of FIs are integrated with published direct measurements of hydrothermal fluids on the Mohns Ridge and both direct and FIs measurements on the MAR. The present study discusses data on the morphology and FIs analysis of barites collected from hydrothermally altered (hydrothermal) sediments with the primary aim of improving the understanding of the genetic aspects and local physicochemical conditions for the formation of sulfate–sulfide deposits on the Mohns Ridge, the sector of the northern Mid-Atlantic Ridge extending beyond the Arctic Circle latitude (66° N).

2. Geological Setting

Depending on the source rocks and the geological setting, the compositions of the sulfide–sulfate deposits can vary considerably [40]. The geological setting where barite forms determines the geochemistry of the precipitated mineral and its usefulness for various applications [1]. The Mohns segment of the ultraslow-spreading Arctic Mid-Ocean Ridge (AMOR) between 71.2°N and 73.5°N with 16 $\text{mm}\cdot\text{yr}^{-1}$ full *spreading rate* [41] is a ~600 km long that extends from the Jan Mayen Fracture Zone to the Knipovich Ridge in the Norwegian–Greenland Sea. A characteristic structural features of the Mohn Ridge are axial volcanic ridges (AVRs) located inside its rift valley [42]. AVRs are strong indicators for underlying heat source whose heat transfer plays a major role in hydrothermal circulations. On the Mohns Ridge, the AVRs are oriented in azimuth 30–35° suborthogonally to the spreading direction, while the rift valley extends in the direction of 60° [43–45].

Research into the geology, geochemistry and biota of the various hydrothermal fields in the Mohns Ridge began in 2005 [32,46]. A feature of the Mona Ridge is the presence of active hydrothermal fields at different depths of the rift valley, varying in terms of fluid temperature (from ~20°C to 320°C) and mineral composition (from nonmetallic vent fields to polymetallic ore-rich deposits) what are developed on bare mafic substrate. The magma chambers located beneath these chimneys have temperatures of around 1,100–1,200 °C [13,37].

Therefore, several active areas of vents have been discovered and studied in the Mohns Ridge: (i) at upper bathyal (from 550 to 724 m) depths – the Jan Mayen vent field area at 71º N; (ii) at deep bathyal (from 2,200 to ~3,000 m) depths – the Loki's Castle, AEgir and Fåvne sulfide vent fields at 72–73º N [32, 33,34,37,38,47,48,49, and references therein]. The active areas of vents are usually located at the floor of the rift valley and related the large axial volcanic ridges (AVRs). In addition to the active fields, several inactive sites with associated seafloor massive sulfide deposits were discovered along the Mohns Ridge, e.g., Copper Hill at 900-m depth, Gnitahei deposit at ~3,000-m depth and Mohns Treasure at 2,600-m depth at 72–73º N [32,37,50].

The southernmost segment of the Mohns Ridge is affected by the Iceland and Jan Mayen hotspots and is characterized by anomalously high magmatic activity, over-thickened crust and shallow water depths [48,51]. Several active low-temperature hydrothermal fields have been discovered in 2005–2014 on the Jan Mayen AVR summit at a relatively shallow depth [32,37], namely: Troll Wall, Soria Moria I and II, Pearl & Bruce, and the inactive Gallionella Garden vent field. All of these fields are collectively referred to as the Jan Mayen vent fields, and the shallow southernmost part of the ridge is termed the Jan Mayen vent field area [52]. Unique deposits of ferromanganese crusts (Fe-Mn crusts) were also found and sampled within the vent field area. The rare earth elements (REE) abundance, positive Eu anomaly, high ε_{Nd} values, and low $^{87}Sr/^{86}Sr$ ratios in the crust are indicative of the fact that the ore material mainly originated from hydrothermal solutions [53].

The northernmost segment of the Mohns Ridge is characterized by less magmatic activity and crustal thickness then southern segment of the ridge, also spreading centers and rift valleys become deeper and more pronounced, and low-angle detachment faults with up to ~10 km displacements are locally developed [52]. The active Loki's Castle vent field was first discovered in 2008 [32]. This high-temperature black smoker vent field associated seafloor massive sulfide deposits. Dome-shaped core complexes that locally expose lower crustal and upper mantle rocks occur on the western flank of the AVR, whereas the eastern flank is covered by sediments belonging to the distal parts of the Bear Island Fan [33,37].

3. Materials and Methods

3.1. Study area

Bathymetric data of the Mohns Ridge, collected by IO RAS during the 75th cruise of the RV *Akademik Mstislav Keldysh* in 2019 [54], allows us to distinguish 15 AVRs in the Mohns rift valley. Among them, the Jan Mayen AVR is the largest and is located near the Jan Mayen hotspot [51], which is one of the most active areas of submarine neo-volcanism in the ocean.

The sediment samples considered in this work for FIs study were obtained at three stations within the Jan Mayen vent field area (Figure 1b, left inset). Station 6137 was located at the base of the rift valley slope, station 6131 and 5516 – on one of rift valley normal scarps, all of them are near by the Troll Wall vent field (Figure 1c). Station 3146 was subjected to the Perle & Bruce vent field and located at a distance of about 2 km northeast of the Fe-Mn crust field [53] (Figure 1b, left inset). The samples of station 6147 (Figure 1b, right inset and Figure 1d) were directly obtained within the Loki's Castle vent field confined to a rift at the AVR top [33].

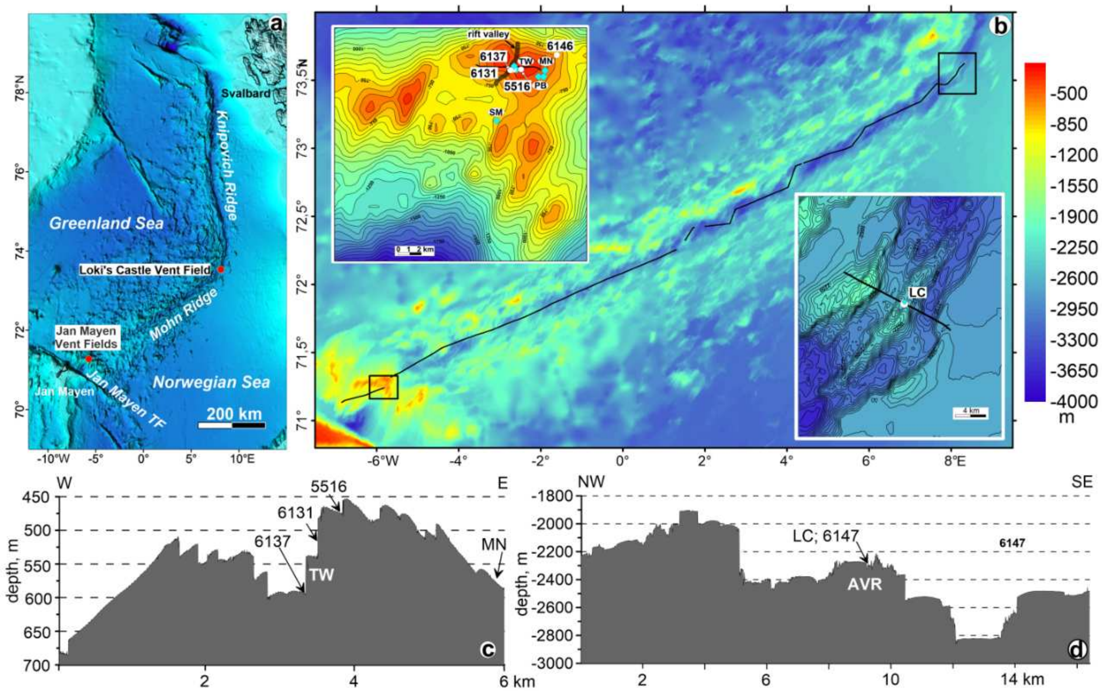

Figure 1. General location of the Mohns Ridge, Jan Mayen Vent Fields and Loki's Castle field (**a**); bathymetric map of the Mohn Ridge and location of the hydrothermal activity areas (boxes) (**b**); the upper left inset shows a bathymetric map of the Jan Mayen AVR top and location of Soria Moria (SM), Gallionella Garden (GG), Troll Wall (TW), Perle & Bruce (PB) hydrothermal fields and Fe-Mn crusts field (MN) (filled blue circles), sampling stations considered in this article are shown by numbered filled white circles; lower right inset shows a bathymetric map of the AVR with the Loki's Castle (LC) hydrothermal field. Grid GEBCO was used for maps preparation; bathymetric profile illustrating the morphology of the Jan Mayen AVR top with the position of the vent fields and stations (**c**); bathymetric profile through the AVR and location the Loki's Castle hydrothermal field and station 6147 (**d**).

3.1.1. Jan Mayen AVR at 71°18' N and related hydrothermal systems

The rift valley trends in the direction of 20–25° dividing the Jan Mayen AVR summit into its NW and SE segments. The north-western and south-eastern walls of the rift valley are bounded by 2–3 scarps of 40–75 m high. Scarps are 10–30 m high, oriented parallel to the rift valley, and are also observed on the NW and SE summit wings (Figure 1b, left inset and Figure 1c). The scarps correspond to the normal faults that limit the steep sides of tilted blocks – structural elements typical for extension conditions.

The Troll Wall vent field is occupied the south-eastern rift wall and situated within a 150-m-deep, 2-km-wide NE-SW-trending rift graben, which transects a large central volcano [48]. The venting occurs through talus deposits at the base of the wall of a rift-bounding normal fault. Venting up to ~270 ºC takes place at a relatively shallow (~550 m) depth and gives rise to numerous active white smoker chimneys [32]. Diffuse low-temperature hydrothermal fluids emanate from ridge parallel faults and fissures along the central rift floor approximately 500 m west of the active relatively high-temperature venting area [55]. The temperature of the diffuse fluids is 2–7 ºC above the ambient seawater temperature (–0.4 ºC).

The Perle & Bruce vent field is located away from the rift valley on the flank of the SE segment of the AVR summit, which is cut by normal faults. An active outflow of fluid occurs along one of the normal faults parallel to the rift valley. That field is characterized by the presence of a hydroacoustic anomaly caused by the release of gas into the water column [34]. Unique deposits of Fe-Mn crusts were discovered and sampled within the Jan Mayen vent field area in the vicinity of Perle & Bruce vent field (Figure 1b, left inset and Figure 1c). The REE composition, positive Eu anomaly, high εNd values, and low 87Sr/86Sr ratios in the crust are indicative of the fact that the ore material mainly originated from hydrothermal solutions [53]. The high-temperature endmember fluids up to 242 ºC venting through the hydrothermal chimneys. The diffuse venting (<54 °C) emanating from the surrounding mound sediments and is evidently derived from the Bruse endmember fluid [56].

3.1.2. The AVR at 73°30' N and 8° E and related hydrothermal system

The Loki's Castle vent field has been discovered since 2008 [32]. The vent field is located on the AVR consisting of hydrothermal debris from previously collapsed structures in the Mohns-Knipovich bend in the area where is a sharp bend in the axial zone of the Mohns Ridge in the northern direction (Figure 1a). The AVR's length equal 30 km and the width is 4 km; it is located in the central part of the rift valley, the width of which is 8.5 km here (Figure 1b, right inset).

The rift corresponds to depression outlined with a contour line of 2300 m. Rift walls with a height of 50–100 m are distinguishable at the bathymetric profile obtained in 75th cruise and crossing the Loki's Castle vent field (Figure 1d). The vent field consists of four active sulfide chimneys up to 13 m high apparently associated with two sub-parallel normal faults that extend in a northeasterly direction and limit the rift north-western side [32,52]. The vent field located on top of two sulfide mounds, forming a composite mound with a size comparable to that of the Trans-Atlantic Geotraverse (TAG) mound (26°08′N on the Mid-Atlantic Ridge) [37,57]. Even though the active chimneys have grown on a basaltic ridge, geochemical fluid data show a strong sedimentary influence into the hydrothermal circulation at the Lokí's Castle [33] due to close location to the Bear Island sediment fan. The hydrothermal field is venting up to 300–320 ºC hot black smoker fluids. Additionally, a low-temperature (~20 ºC) vent area featuring numerous small barite-silica chimneys occurs adjacent to the eastern mound [13].

3.2. Field Observations and Sample Collection

CTD profiling using Seabird SBE911plus (Sea-Bird Electronics, Inc.) was performed in order to document the ambient seawater properties. Buoyant plume particles were collected using cylindrical sediment traps deployed at a depth of 30 m from the seafloor [58].

Mineralized and hydrothermally altered sediments were collected by the grab (0.25 м^2 sampling area) from the Jan Mayen vent field area at 71º N within the Troll Wall and Perl & Bruce vent fields and the Loki's Castle vent field at 73º N, during the 68th and 75th cruises of the RV *Akademik Mstislav Keldysh* in July 2017 and June 2019, respectively [54,59] (Figure 1). Five different sulfide-rich *samples were investigated on-board and immediately* dried at 30 °C prior to father procedures. All the samples were examined using a Carl Zeiss Stemi 508 binocular microscope. The types of sediment were determined according to the Bezrukov and Lisitzin [60] classification of sea bottom sediments [61].

The bathymetric and hydroacoustic investigations were performed with a Kongsberg EA600 ship-mounted single-beam echosounder operating at a constant frequency of 12 kHz. The standard software EA600 was used to control the echosounder. Hydroacoustic and bathymetric surveys were performed in the studied areas along the separate transects.

3.3. Petrography and Mineralogy

All samples were examined for purity by X-ray diffraction (XRD) and scanning electron microscopy (SEM) with energy-dispersive spectrometry (EDS). The composition of the sulfide-rich *samples* was studied in bulk and hand-picked aggregates and grains. Sub-samples were finely crushed in an agate mortar and the same 'bulk' powder was used for X-ray diffraction (XRD). The list and abundance of hydrothermally derived minerals is represented in Table 1.

Table 1. List of identified hydrothermally derived minerals and their abundances in the studied assemblages from the sediments of the Troll Wall, Perle & Bruse and Loki's Castle. Mineral abundance: Major – identified in most samples examined, including bulk, fraction >0.63 mm and hand-picked aggregates; Minor – identified regular in hand-picked aggregates or grains; Rare – identified episodically in hand-picked aggregates or grains.

Mineral	**Formula**	**Abundance**	**Content range, wt. %**
Troll Wall, proximal sediments			
Smectite (partially hydrothermal)	$M^{+}_{x+y}(R^{3+}_{2-y}\ R^{2+}_{y})(Si_{4-x}\ Al_{x})\ O_{10}\ (OH)_{2} \cdot nH_{2}O$	Major	15–62
Fe-Si oxyhydroxides	Fe amorphous silica	Major	n.d.
Barite	$Ba(SO_4)$	Major	3–85
Gypsum	$CaSO_4 \cdot 2H_2O$	Major	1–11
Pyrite	FeS_2 (cubic)	Major	4–99
Marcasite	FeS_2 (rhombic)	Major	4–87
Sphalerite	ZnS	Major	1–10
Chalcopyrite	$CuFeS_2$	Minor	1–2
Bernessite	$(Na,Ca)_{0.5}(Mn^{4+},Mn^{3+})_2O_4 \cdot 1.5H_2O$	Minor	n.d.
Buserite I	$Na_4Mn_{14}O_{27} \cdot 21H_2O$	Minor	n.d.
Asbolane– Buserite	mixed-layer Mn formation	Minor	n.d.
Chlorite–smectite	mixed-layer cay formation	Minor	0–37
Wurtzite	(Zn,Fe)S	Rare	2–5
Goethite	α-FeO(OH)	Rare	1–53
Lepidocroquite	γ-FeO(OH)	Rare	0–25
X-ray *amorphous clay*	ultrafine structurally defective clay formation	Rare	n.d.*
Mordenite	$(Na_2,Ca,K_2)_4(Al_8Si_{40})O_{96} \cdot 28H_2O$	Rare	0–93
Jarosite	$KFe^{3+}_3(SO_4)_2(OH)_6$	Rare	13
Perle & Bruse, distal sediments			
Smectite (partially hydrothermal)	$M^{+}_{x+y}(R^{3+}_{2-y}\ R^{2+}_{y})(Si_{4-x}\ Al_{x})\ O_{10}\ (OH)_{2} \cdot nH_{2}O$	Major	n.d.
Barite	$Ba(SO_4)$	Major	1–6
Gypsum	$CaSO_4 \cdot 2H_2O$	Major	1–6
Bernessite	$(Na,Ca)_{0.5}(Mn^{4+},Mn^{3+})_2O_4 \cdot 1.5H_2O$	Major	n.d.
Buserite I	$Na_4Mn_{14}O_{27} \cdot 21H_2O$	Major	n.d.
Fe-oxydes	Fe_2O_3	Major	n.d.
Pyrite	FeS_2 (cubic)	Minor	1–2
Smectite–illite (partially hydrothermal)	mixed-layer clay formation	Rare	2–4
Buserite II	$Na_4Mn_{14}O_{27} \cdot 21H_2O$, heat resistant	Rare	n.d.
Asbolane	$(Ni, Co)_{2-x}Mn^{4+}(O, OH)_4 \cdot nH_2O$	Rare	n.d.
Asbolane–Buserite	mixed-layer Mn formation	Rare	n.d.
Loki's Castle, proximal sediments			
Smectite (mostly hydrothermal)	$M^{+}_{x+y}(R^{3+}_{2-y}\ R^{2+}_{y})(Si_{4-x}\ Al_{x})\ O_{10}\ (OH)_{2} \cdot nH_{2}O$	Major	10–30
Talc	$Mg_3Si_4O_{10}(OH)_2$	Major	1–95
Pyrite	FeS_2 (cubic)	Major	3–18
Pyrrhotite hexagonal	$Fe\ nS_{n+1}$	Major	5–81
Chalcopyrite	$CuFeS_2$	Major	2–75
Sphalerite	ZnS	Major	2–13
Barite	$Ba(SO_4)$	Major	2–28
Sulfur native	S	Major	4–34
Goethite	α-FeO(OH)	Major	3–18
Chlorite–smectite	mixed-layer clay formation	Minor	n.d.

Pyrrhotite monoclinic	$Fe\ nS_{n+1}$	Minor	5–15
Marcasite	FeS_2 (rhombic)	Minor	3–30
Lepidocroquite	ɣ-FeO(OH)	Minor	1–24
Gypsum	$CaSO_4 \cdot 2H_2O$	Minor	1–8
Talc-like mineral–smectite	mixed-layer formation with Mg-Fe phyllosilicate	Minor	n.d.
Galenite	PbS	Rare	2–3
Famatinite	Cu_3SbS_4	Rare	0–4
Paratacamite	$Cu_3(Cu, Zn)(OH)_6Cl_2$	Rare	0–58
Jarosite	$KFe_3^{3+}(SO_4)_2(OH)_6$	Rare	0–35

*n.d. – not detected.

Detailed mineralogical identification by XRD was performed on unoriented prepared specimens analyzed by a Bruker D8 Advance diffractometer (BRUKER AXC, Germany) (Cu K_α with Ni 0.02 filter, 40 kV, 40 mA, with a linear detector LYNXEYE with scanning in a discrete mode with a 0.02 °steps, exposure 4 seconds/step in a range of 2.5°–70° 2θ range) in IO RAS. Mineral identification was performed with an automatic/manual peak search using BRUKER's Diffrac EVA 3.1. The PDF4 Mineral database of ICDD and the Crystallographic Open Database (COD) were used for identification purposes. Mineral quantification was performed by Rietveld refinement using the TOPAS 5 *software.*

Separate subsamples were examined using a VEGA-3sem TESCAN (Czech Republic) scanning electron microscopy (SEM) with an energy dispersive X-ray spectrometer (EDS), Oxford INCA Energy 350 (United Kingdom). Polished thin-sections from representative samples were selected for EDS analyses of specific barite mineral phases.

3.4. XRF Analysis

X-ray fluorescence (XRF) analysis of 'bulk' powder sediment samples impacted by hydrothermal alteration and hyaloclastites was performed on a sequential spectrometer with wavelength dispersion, model Axios mAX (PANalytical, Netherlands), and software SuperQ (PANalytical). For the rock-forming oxide analyses, preparations were made from sample powder dried at 110ºC by melting with a mixture of lithium borates at 1150 ºC. Glassy disks were formed from the resulting borate melt and analyzed on a spectrometer. To determine trace elements and sulfur, preparations were made from the sample powder by cold pressing with plastic filler at 30 tons pressure into 32 mm diameter tablets, which were analyzed on a spectrometer. XRF major element composition of the sediment samples is given in Supplementary material (Table S1). The analysis was conducted in order to reveal the type of studied sediments and asses the metalliferous sediment index (MSI).

3.5. Sample Preparation and Fluid Inclusions Petrography

Fluid inclusion studies were performed using zoned barite crystals of 1,000–100 µm in size (Figure 2a) collected from sulfide-rich assemblages from the Troll Wall (sample 6131), Perl & Bruce (sample 6137) and Loki's Castle (samples 6146–6147) seafloor sulfide deposits. Barite was separated from other minerals using the optical microscope Olympus BX51. FIs used for measurements ranged in size from 5 µm to 15 µm in length. The most common size was between 8 µm and 15 µm. The microthermometric study was conducted on carefully selected FIs with no evidence of necking-down or leakage. At room temperature all studied FIs contain a liquid phase and a vapour bubble.

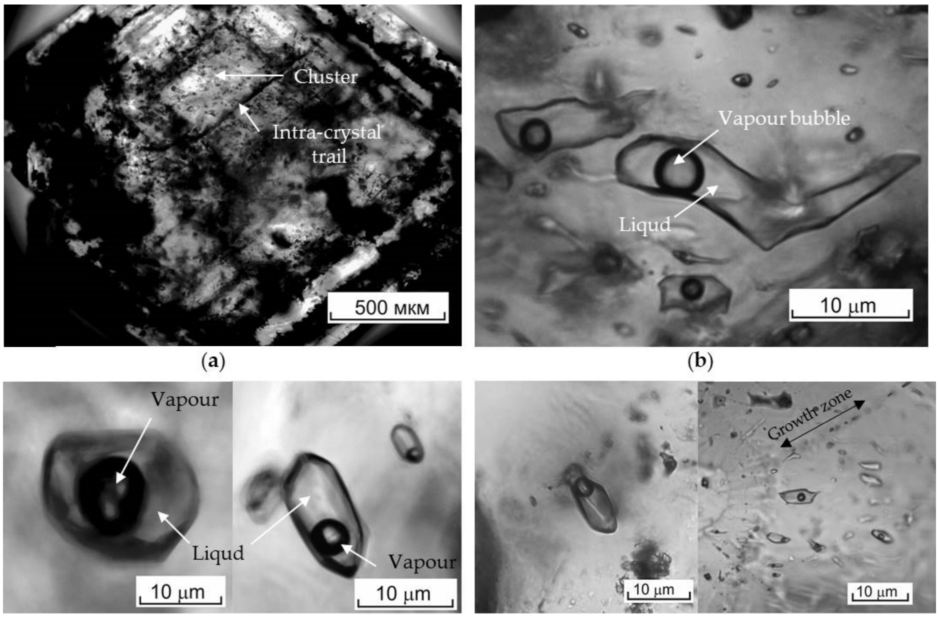

(**a**) (**b**)

(**c**) (**d**)

Figure 2. Micrographs of zoned barite crystal (**a**) and two-phase liquid-vapor fluid inclusions (**b–d**) in barite crystals.

Three textural generations of FIs were observed within the barite crystals: (1) presumed primary (P), (2) primary-secondary (P–S), and (3) secondary (S) inclusions. Primary two-phase liquid-vapor FIs occurring within barite crystals were just one type with a vapor bubble occupying less than half the volume of the inclusion (volume of the vapour phase: 15–20 vol. %), and an liquid solution (Figure 2 b–d). The observed FIs have a negative crystal shape. The primary origin of the FIs is determined according to the criteria proposed in Roedder [35]. Therefore primary FIs are confined to growth zones or uniformly distributed in the host mineral volume, primary-secondary FIs are confined to fractures not extending beyond barite crystals boundaries, and secondary FIs are localized in secant fractures.

3.6. Fluid Inclusions Microthermometry

The FIs studies were carried out at the Department of Geochemistry of the Institute of the Geology of Ore Deposits, Petrography, Mineralogy, and Geochemistry (IGEM), Russian Academy of Sciences, on a Linkam THMSG600 (United Kingdom) heating–freezing stage mounted on an Olympus BX51 microscope and video camera. The above measuring setup allows real-time measurements to be made of the temperature of phase transitions in the inclusions in the range from –196 ºC to 600 ºC and to observe them at high magnifications and make digital microphotos. Calibration of the heating–freezing stage was carried out using SYN-FLINC® synthetic fluid inclusion temperature standards. Microthermometric measurements was calibrated against the CO_2 triple point and H_2O (ice) melting point.

The salt concentrations (salinities, reported as wt.% NaCl eq.) of liquid in FIs was calculated from the dissolution temperature of the ice crystal, using data from the work of [62]. The salt composition of the liquid in FIs was determined by eutectic temperatures according to [63]. Salinities and liquid densities, as well as calculations of temperature corrections for pressure and trapping temperatures of FIs, were inferred using the software "FLINCOR" [64]. The $T_{ice\ melt}$ and T_{hom} were determined with a precision of ±0.1 °C and ±1 °C, respectively. Crystallization or trapping temperatures (T_{cryst}) were determined by applying a hydrostatic pressure correction to the homogenization temperatures (T_{hom}), which is defined as the minimum temperature in which a single phase fluid is present in the inclusion. Pressure correction (P = 239 bar) was made assuming 2376 m water depth at Loki's Castle vent field, 1025 kg/m^3 seawater density, and the addition of 1 atm of air pressure above the sea. Consrquently, the pressure correction for the Jan Mayen vent fields was 70 bar. The results of microthermometric measurements are given in Table 2.

Table 2. Fluid inclusion data for the Troll Wall, Perl & Bruce and Loki's Castle seafloor sulfide deposits.

Station, depth, layer	Type of FIs*	n	T_{hom}, °C	T_{eut}, °C	$T_{ice\ melt}$, °C	Salinity, wt.% NaCl eq.	*d*, g·cm^{-3}	*T***, °C	T_{cryst}***, °C
Troll Wall vent field, depth of 512–600 m									
6131 512 m 0–20 cm	P	8	275	-33	-2.1	3.4	0.80	1	276
	P	4	246	-31	-2.3	3.8	0.84	3	249
	P	4	218	-33	-2.5	4.1	0.88	3	221
	P	5	217	-31	-2.6	4.2	0.88	3	220
	P-S	3	195	-31	-2.5	4.1	0.90	3	198
	P-S	2	167	-25	-2.5	4.1	0.93	4	171
	S	2	115	-27	-2.3	3.8	0.98	4	119
6131 512 m 1–9 cm	P	7	264	-33	-2.6	4.2	0.82	2	266
	P	6	234	-32	-2.1	3.4	0.85	3	237
	P	5	234	-32	-2.1	3.4	0.85	3	237
	P	8	216	-31	-1.9	3.1	0.87	3	219
	P	6	215	-34	-2.1	3.4	0.88	3	218
	P-S	5	186	-33	-2.1	3.4	0.91	4	190
	S	3	156	-34	-1.9	3.1	0.94	4	160
	S	6	156	-32	-1.7	3.1	0.94	4	160
6137 600 m 0–5 cm	P	8	234	-33	-2.5	4.1	0.86	3	237
	P	6	231	-34	-2.4	3.9	0.86	3	234
	P	7	230	-32	-2.3	3.8	0.86	3	233
	P	4	223	-30	-1.9	3.1	0.86	3	226
	P	10	219	-32	-1.7	2.8	0.87	3	222
	P	6	218	-30	-2.2	3.6	0.87	3	221
	P	5	213	-34	-2.0	3.3	0.88	3	216
	P	7	211	-33	-2.2	3.6	0.88	3	214
	P-S	5	193	-31	-2.0	3.3	0.90	4	197
	P-S	5	166	-32	-2.1	3.4	0.93	5	170
	P-S	3	161	-33	-2.1	3.4	0.93	4	165
	S	4	159	-30	-1.8	3.0	0.93	4	163
5516 540 m 0–3 cm	P	3	260	-35	-1.9	3.1	0.81	2	262
	P	2	257	-30	-2.0	3.3	0.82	3	260
	P	2	257	-34	-2.7	4.4	0.83	3	260
	P	16	247	-33	-2.0	3.3	0.83	3	250
	P	3	243	-31	-2.5	4.1	0.85	3	246
	P	5	243	-32	-1.9	3.1	0.84	3	246
	P	3	241	-31	-1.9	3.1	0.84	3	244
	P	2	240	-32	-1.6	2.6	0.84	3	243
	P	2	235	-32	-2.1	3.4	0.85	3	238
	P	4	226	-32	-2.2	3.6	0.86	3	238
	P	8	209	-30	-2.0	3.3	0.88	3	212
	P	3	203	-32	-2.1	3.4	0.89	3	206
	P	5	199	-31	-2.3	3.8	0.90	4	203
	P	5	198	-33	-2.6	4.2	0.90	4	202
	P	4	186	-33	-1.8	3.0	0.91	4	190
	P	2	128	-30	-1.8	3.0	0.96	4	132

Perl & Bruce vent field, depth of 620 m									
6146	P	3	271	-30	-2.3	3.8	0.80	2	273
620 m	P	4	266	-34	-2.4	3.9	0.81	2	268
0–9 cm	P	6	263	-32	-2.3	3.8	0.81	2	265
	P	4	249	-31	-2.5	4.1	0.84	3	252
	P	3	248	-31	-2.1	3.4	0.83	3	251
	P	3	247	-27	-2.1	3.4	0.83	3	250
	P	6	238	-34	-2.4	3.9	0.85	3	241
	P	7	236	-32	-1.9	3.1	0.83	3	239
	P-S	4	225	-33	-2.3	3.8	0.87	3	228
	P-S	5	211	-32	-2.0	3.3	0.88	3	214
	P-S	2	184	-30	-2.6	4.2	0.92	4	198
	S	3	135	-28	-2.2	3.6	0.96	4	139
Loki's Castle vent field, depth of 2376 m									
6147	P	13	287	-32	-2.6	4.2	0.78	20	307
2376 m	P	4	281	-35	-1.8	3.0	0.77	20	301
0–12 cm	P	7	273	-32	-2.2	3.6	0.79	20	293
	P	2	265	-31	-2.7	4.4	0.82	20	285
	P	4	261	-33	-2.1	3.4	0.81	20	281
	P	5	256	-34	-1.9	3.1	0.82	20	276
	P	6	253	-33	-1.8	3.0	0.82	20	273
	P	2	251	-33	-2.3	3.8	0.83	20	271
	P	3	244	-30	-2.3	3.8	0.84	19	263
	P	9	234	-35	-2.6	4.2	0.86	19	253
	P	6	228	-34	-2.1	3.4	0.86	19	247
	P-S	2	227	-30	-1.9	3.1	0.86	19	246
	P-S	6	219	-31	-2.4	3.9	0.88	18	237
	P-S	7	218	-31	-2.1	3.4	0.87	18	236
	P-S	5	214	-33	-2.2	3.6	0.88	18	232
	P-S	7	205	-32	-1.7	2.8	0.88	18	223

*Genetic types of FIs: P – primary, P-S – primary-secondary, and S – secondary. n – number of FIs. **Pressure correction: Troll Wall – ~59 bar, Perl & Bruce – 61 bar, and Loki's Castle – 233 bar. ***T_{cryst} of hosted mineral (fluid trapping temperature).

4. Results

4.1. Temperature and Salinity of Ambient Seawater

Most of the water column from the seafloor to layer of ~140 m in the Jan Mayen vent field area is occupied by cold Arctic intermediate water with temperatures and salinity of –0.27–0.3 °C and 34.88–34.91 psu, respectively. Only the upper quasi-uniform layer of about 0–60 m is warmed till 2–3 °C. The measured ambient seawater temperature varied from –0.27 °C to –0.19 °C and from –0.13 °C to –0.10 °C at different depth ranges: 774–660 m and 600–550 m, respectively. Positive temperature anomalies were recorded within the buoyant hydrothermal plumes where the temperature reached 0.64–2.49 °C.

In the area of the Loki's Castle vent field, the deep water mass of ~1500 m thickness is occupied by cold Arctic intermediate water with sub-zero temperatures and salinity of 34.91 psu. The upper quasi-uniform layer 0–60 m is warmed to 5.59 °C. The measured ambient seawater temperature reaches –0.72 °C at a depth of 2368 м. Therefore the ambient temperatures varied from –0.10 °C till –0.72 °C and depend of the depth of the vent fields. The ambient salinity is approximately 34.91 psu at both locations that is 31.85 psu NaCl eq.

4.2. Petrography and Lithology

Mineralized and hydrothermally altered sediments of variable thickness layer are rest on a substrate composed primarily of silicified hyaloclastite and basaltic debris. Boulders of hyaloclastites and basalts, as well as, breccia are widespread on the seafloor of the Jan Mayen vent field area. Volcanic tuffs (~15 × 10 × 5 cm) from dark brown to black colors were collected in this area, containing on the surface fragments of shells, glandular crust, and organic matter residues.

Hydrothermal sediments of the Troll Wall vent field are coarse- and medium-grained dark gray tuffaceous sands with inclusions of basalt lithoclasts (medium and fine rubble), ferruginous tuffs, and psammite, siltstone, and mudstone breccia sized 1–8 cm often with a ferrous film on the surface. Sands contain lapilli-size volcanic fragments, bright brown ferruginous crusts-like fragments and red spots of ferrugination at the surface. and characteristic signs of hydrothermal alterations in form of white and gray fluffy clay. Fragments of rocks, shells, and pebbles (4 × 3 cm) are present as well. Beneath the thin (~1 cm) oxidized surface layer of the sediment, a patchy sediment texture with reddish-gray compaction appears, probably along zones of diffuse fluid penetration. The sands are weakly iron-rich (5 to 10 wt.% Fe according to [61]), with an average Fe content of 8±0.9 wt.% in the studied samples.

Hydrothermal sediments of the Perle & Bruce vent field are medium- and fine-grained tuffaceous dark grayish-brown sands with basalt inclusions (fine rubble); psammite structure. Beneath the thin (~1 cm) oxidized surface layer, a spotted texture appears on the background of a very dark grayish-brown or brown sediment. The influence of regular pelagic marine sediments at the Perl & Bruce vent field is more significant than at the the Troll Wall vent field. In terms of iron content, the sands are usually weakly iron-rich, with an average Fe content of 6±0.1 wt.%, but ferruginous (10–20 wt.% Fe) with an average Fe content of 14.5±0.2 wt.% and weakly manganese (5–0.2 wt.% Mn) with an average Mn content of 0.35±0.1 wt.% sands was also collected.

Hydrothermal sediments of the Loki's Castle vent field are coarse unsorted muddy sands; psammite structure. The top layer (0–6 cm) is brown sands with ochreous, yellow and black grains, many ochreous crusts-like agglomerates up to 3 cm, and white fluffy clay on the surface of the agglomerates. Deeper (6–12 cm) are oblique layers of dark reddish-brown colour, as well as areas of very dark greyish-brown colour. Close to the base of the exposed sand layer, dense agglomerates are often covered with cubic pyrite crystals. The texture of the sediment is pseudo-agglomerate, spotty-layered and heterogeneous with sharp boundaries. Fluid conduits were observed in a regular circular shape up to ~10 cm in diameter with sharp boundaries and denser bluish-grey sediment inside. There were fine quartz and feldspar grains, obviously ice-rafted debris, coated with an iron film. In terms of iron content, the sands are weakly iron-rich (9 wt.% Fe) and ferruginous (>10 wt.% Fe).

Basaltic rocks are present in hydrothermal systems, the Jan Mayen and Loki's Castle vent fields. On the rift wall occupied by Troll Wall, volcanic tuff and semi-lithified volcaniclastic psammite breccia (more than 70% of volcanic glass) was mostly collected. Volcanic breccia is polymictic of dark gray and bluish color with ochre-colored and black-colored interlayers and contains fine pebbles and gravel and inclusions of gray silt nodules. The volcanic breccia often has sings of hydrothermal alteration and mineralization: sulfide crystals (dominantly cubic pyrite), barite and Fe-Si oxyhydroxides. The basaltic and glassy fragments are widespread in the surface sediments of the Troll Wall and Perle & Bruse vent fields. Basalt lithoclasts of wide size (till 5 cm) and often angular and subangular shape are characterized by a vesicular structure with porphyritic and microporphyritic texture, dominated by volcanic glass and, in smaller amounts, containing split phenocrysts of plagioclase and idiomorphic phenocrysts of clinopyroxene and olivine (Figure 3). The volcanic glass in these samples differs in the degree of alteration: from colourless, transparent and dense, to light yellow and fractured, with areas of palagonite (altered glass) and smectite, to a black isotropic opaque mass composed entirely of smectite microfibers.

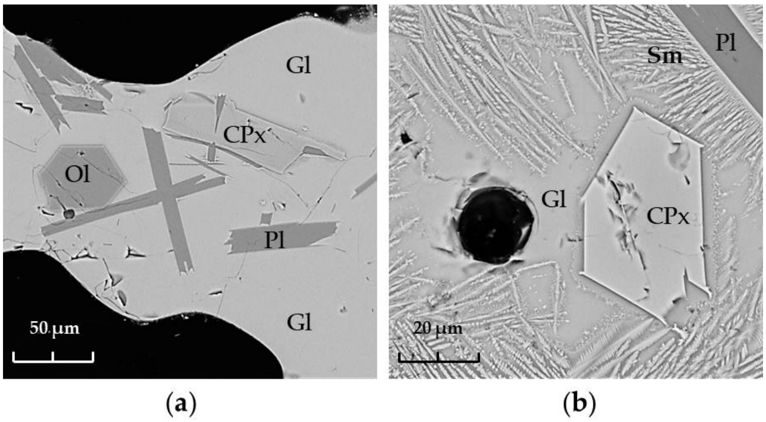

(**a**) (**b**)

Figure 3. SEM micrographs of volcanic glasses with phenocrysts and p*alagonisation*: Gl – glass, CPx – clinopyroxene, Pl – plagioclase, Ol – olivine, Sm – smectite.

Glassy pillow basalts and occasional glass fragments were detected in the surface sediments of the Loki's Castle vent field. Basalt lithoclasts are characterized by sparsely phyric texture, dominated by volcanic glass, small amounts of plagioclase and olivine phenocrysts and less frequently pyroxene phenocrysts. Yellow and light brown glass characterized by altered areas with palagonite and ochre microfibers. Coarse (1–4 cm) angular shards of black glass, usually with ochre film, were collected from the surface of soft sediments in the proximal area of the vent field. The isotropic opaque glass shards demonstrate curving fracture rims, typical of conchoidal fracture.

Crust-like orange-ochre, yellow-ochre, yellow, dark red, and black agglomerates are occur in the volcanic breccia and sediments of the studied Jan Mayen vent fields. Matrix of the ochre-colored crusts is represented by collomorphic Fe-oxydes, yellow colored or dark red – usually by Fe-Si oxyhydroxides, and black – by collomorphic Fe and Mn oxyhydroxides. The newly discovered Fe-Mn crusts in the distal area of the Perle & Bruse vent field [53] is layered slabs (up to ~3 cm thick, and ~25 × 12 cm in size) composed of homogeneous ore matrix of Mn and Fe oxyhydroxides with an admixture of non-metallic matter, mainly fine-dispersed volcanic glass. The ore matrix consists mainly of Mn hydroxides with a subordinate admixture of Fe-oxydes. Crust-like agglomerates, grains and globules of ochreous, yellow and black colours, represented by Fe-oxides, talc and native sulfur, are found in sediments of the Loki's Castle vent field.

4.3. Mineralogy

XRD data of the Troll Wall sediments indicates plagioclase and smectite (hereinafter following in decreasing order of content) as dominant phases in bulk mineralogy which followed by pyroxene and olivine. Quartz, feldspar and other clay minerals (kaolinite, chlorite and illite) are much less frequently or occur in trace amounts. Mixed-layer clays with swelling layers of chlorite–smectite type, on the other hand, are common in sediments. It has been found that X-ray *amorphous clay* may contain in the surface sediment layer. Sulfides are represented mostly by pyrite and marcasite and less frequently by sphalerite, chalcopyrite and wurtzite. Cu and Zn sulfides are often precipitate deposited as collomorphic textures of sphalerite and chalcopyrite in association of barite. The hydroxide class is mainly represented by Fe-oxides, such as, goethite, lepidocroquite, and Mn-hydroxides, such as, bernessite, buserite I and asbolane–buserite as subordinate mineral. Fe-Si oxyhydroxides (halo in the angular interval 17–30 2θ° with a maximum in range of approximately 4 Å) are found in sediments and form edifices. Mordenite-type *zeolite* was detected in the altered volcaniclastic breccia. Among the sulfate minerals, barite was identified as well as gypsum and jarosite as accompanying minerals. The sediments are rich in barite (till 19 wt.% in bulk mineralogy and till 85 wt.% in aggregates associated with sphalerite), which forms mineral associations with sulfides but does not form chimney edifices.

XRD data of the Perle & Bruse sediments indicates calcite, plagioclase and quartz as dominant phases in bulk mineralogy which followed by pyroxene. Feldspar and clay minerals (kaolinite, chlorite, illite and minor smectite) are much less frequently or occur in trace amounts. Mixed-layer clays with swelling layers of smectite–illite type are also identified in sediments. Sulfides are represented mostly by pyrite. In hydroxide class is dominated by Mn-hydroxides, such as, bernessite, buserite I and asbolane or asbolane–buserite as subordinate minerals. Fe-oxydes are common but do not form their own crystalline mineral phase in sediments. Barite and gypsum are identified among the sulfate minerals (1–6 wt.% in total).

XRD data of the Loki's Castle sediments indicates that the dominant phases are smectite, talc and quartz, followed by plagioclase and calcite. Other clay minerals (kaolinite, chlorite and illite) occur in trace amounts. The sediments reveal mixed-layer clays with swelling layers of chlorite–smectite type and talc-like mineral–smectite type, which according to [38] has been interpreted as talc-like kerolite–smectite of Mg-Fe phyllosilicate type. The former contains fine sphalerite and goethite, the latter fine sulfides such as hexagonal pyrrhotite, chalcopyrite and sphalerite. Sulfides are represented by a wide range of mineral varieties: pyrite, *pyrrhotite* (monoclinic and *hexagonal),* chalcopyrite, sphalerite and less frequently marcasite, galenite and famatinite. The content of sulfide minerals vary from 3 wt.% to 72 wt.% in total mineralogy and different rock fragments of sediments, respectively. Native sulfur is common in studied sediments, most often in the form of globules and as part of aggregate clusters. The hydroxide class is mainly represented by Fe-oxides, such as, goethite and lepidocroquite. The Cu-Zn chloride *mineral*, paratacamite, occur as dark aggregates in association with lepidocroquite and goethite. Among the sulfate minerals, barite, jarosite and gypsum were identified. The sediments are rich in barite (2–15 wt.% in bulk mineralogy), which forms mineral associations with sulfides but does not form chimney edifices in the studied site. Dark-coloured fractions <63 μm are rich in barite up to 28 wt.%.

4.4. Wholerock Composition and Dominant Trace Elements

To reveal the possibility of a non-detrital origin for Si content in the studied sediments, Si was plotted against Al according to Turekian et al. [65] (Figure 4). There are no a pair correlation between Si and Al in that sediments due to high basaltic contribution. The sediments demonstrated a Si/Al ratio varied from 1.3 to 3.9 and most of them were around 3.0 indicative the high input of detrital material (Figure 5a). Perl & Bruce sediments have slightly increased Si/Al ratios: ~3.5 in average. A Si/Al ratio of Loki's Castle sediments reached 25 what confirms the higher value of Si and reflects the high clay component and the igneous mafic nature.

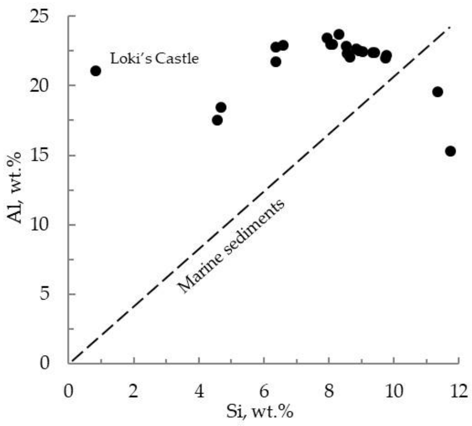

Figure 4. Si versus Al content in the hydrothermally altered sediments.

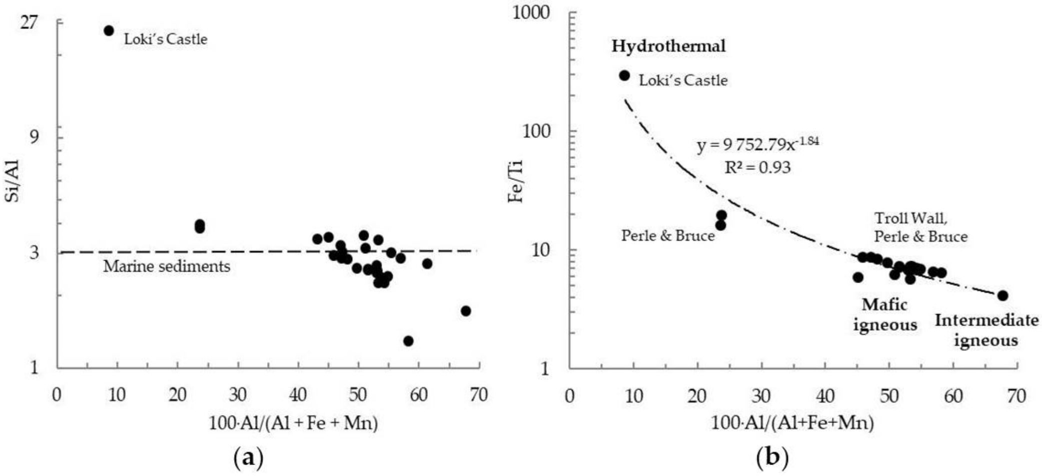

Figure 5. Plot of Si/Al ratio (**a**) and Fe/Ti ratio (**b**) versus metalliferous sediment index after [66] for the hydrothermally altered sediments.

All sediment samples examined have Mn/Fe ratios <0.03 and cannot be classified as metalliferous sediments according to [67], where this ratio must exceed 0.07. The Perle & Bruce sediment samples demonstrate Mn/Fe values of 0.03–0.02 indicative of little diagenetic alteration [68]. The values of Boström et al. [66] metalliferous sediment index, 100·Al/(Al+Fe+Mn), for the Loki's Castle and Perle & Bruce sediments reached 8.7 and 23.7, respectively. Therefore extremely Al-depleted (0.8 wt.%) and Mg-enriched (14 wt.%) sediments of the Loki's Castle reflect the higher Fe content due to a more hydrothermal composition (sulfides and talc). Al-depleted (4.6 wt.%) Fe-Mn-enriched sediments within the Perle & Bruce vent field are approaching distal metalliferous sediments possible reflects the high Fe and Mn oxyhydroxides input. Other Perle & Bruce sediments and all Troll Wall sediments demonstrate the variation of the metalliferous sediment index between 45.8 and 67.8, reinforcing the dominance of the detrital character of the sediments. Most sediment samples from the Perle & Bruce and Troll Wall vent fields exhibit elements indicative of a dominant igneous mafic and intermediate component, in comparison to the Loki's Castle sediments to be essentially influenced by hydrothermal component (Figure 5b).

Ba content in Troll Wall and Perle & Bruce sediments varied from 388 ppm till 8,800 ppm and reached 16,500 ppm in Loki's Castle sediments. Ba versus S_{total} demonstrated reliable linear approximation (R = 0.95, n = 23) for studied sediments indicative of a dominant hydrothermal affinity (Figure 6). S_{total} content reaches 2.6 wt.% and 9.8 wt.% in sediments of Loki's Castle and Troll Wall, respectively.

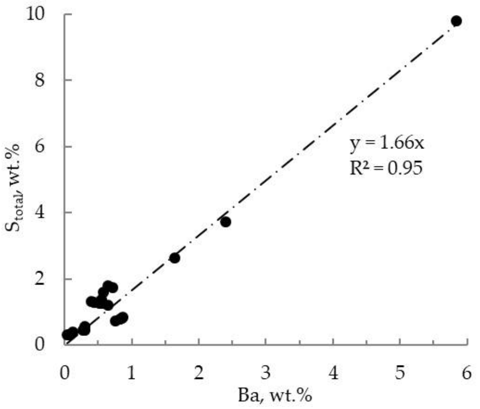

Figure 6. Ba versus S_{total} content in the hydrothermally altered sediments.

In addition to Fe and Mn, three main metals are indicative of hydrothermal alteration, such as, Cu, Zn and Pb. Cu content varied from 58 ppm (which is close to its content in glassy fragments – from 55 to 71 according to Elkins et al. [51] and this work, respectively) to 1,110 ppm in sediment samples of the Troll Wall and Perle & Bruce vent fields. Zn content varied from 57 ppm (which is depleted compared to the average content in glassy fragments – from 104 ppm to 83 ppm according to Elkins et al. [51] and this work, respectively) to 3,140 ppm in sediment samples of the Troll Wall and Perle & Bruce vent fields. The higher Cu and Zn contents are characteristic for the Troll Wall sediments. In Loki's Castle sediment samples, the content reaches 3,600 ppm and 4,800 ppm for Cu and Zn, respectively. Pb content is varied from 18 ppm (which is close to its content in pelagic sediments of 16 ppm [38]) to 109 ppm in sediment samples of studied Jan Mayen vent fields, while its content in basalts is approximately 2 ppm [51]. In Loki's Castle sediment samples, Pb content reaches 2,200 ppm. As and Se are also noteworthy. In Perl & Bruce sediment samples, As content reaches to 211 ppm. In Loki's Castle sediment samples, Se content is as high as 45 ppm.

4.5. Barite Chrystal Morphology, Size and EDS Data

Barite crystals have been found in buoyant plume particles and in sediments from both the Jan Mayen and Loki's Castle vent fields. Flat, micron-sized barite crystals with a crosscutting tabular shape of hexagonal type are identified in the buoyant plume extracted from sediment-trap samples (Figure 7a–c). The tabular crystals form rosette structures in both hydrothermal settings but crystal and rosette sizes vary. In the Jan Mayen vent fields, crystals >10 µm form well-shaped rosettes up to approximately 50 µm and coarse. In Loki's Castle vent field, crystals of 5–10 µm form rosette-like structures up to approximately 15–20 µm. Barite forms mineral associations and aggregates with Fe, Cu, and Zn sulfides. Sulfide minerals form porous as *bud-shaped* masses with individual spherulites of <0.5 µm in size, and only pyrite forms regular octahedrons and cuboctahedrons up to 3 µm in size.

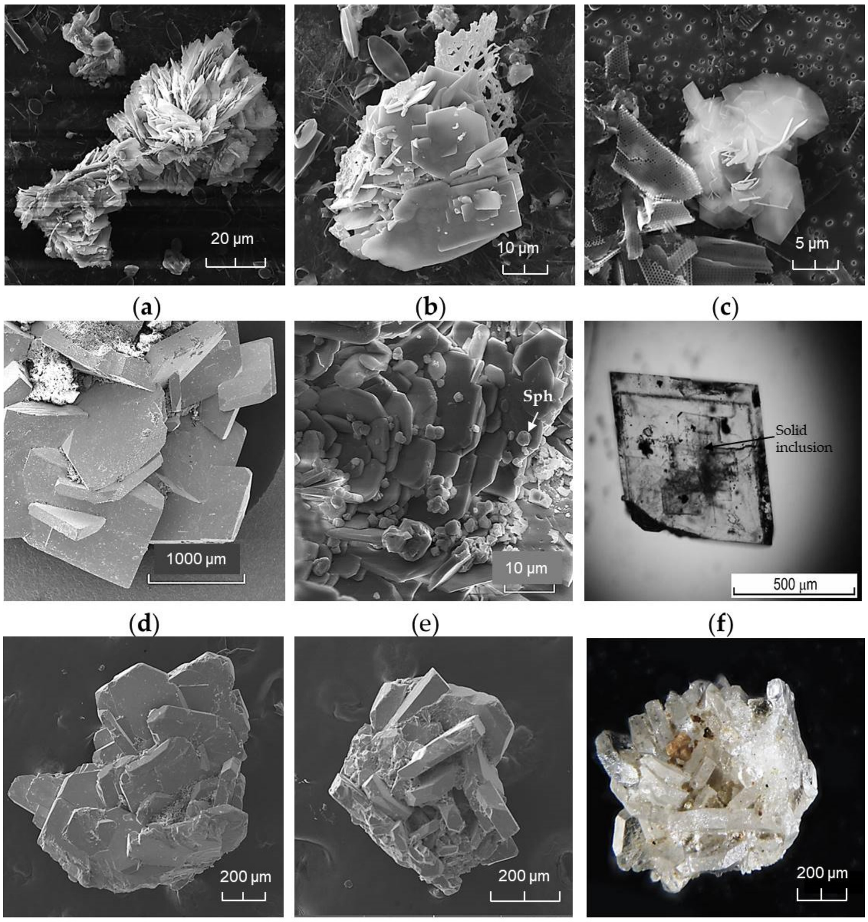

(**a**) (**b**) (**c**)

(**d**) (e) (**f**)

(j) (h) (**i**)

Figure 7. Scanning electron micrographs (**a–e**) and micrograph in plane polarized light (**f, i**) of the barite crystals: (**a,b**) sinking particles from buoyant plume of the Troll Wall vent field; (**c**) sinking particles from buoyant plume of the Loki's Castle vent field; (**d–e**) crystals from surface layer of sediments of the Troll Wall vent field; (**j–i**) crystals from surface layer of sediments of the Loki's Castle vent field. Note: Sph – sphalerite.

In sediments, flat crystals are larger, approximately 20–1,000 µm, and are typically precipitated as tabular shape of hexagonal and rectangular types (Figure 7d–f). Polysynthetic twinning is occasionally found. Idiomorphic crystals typically form rosette and druse structures up to approximately 3 mm and are also often found as individual crystals. There are colourless and clear water crystals, as well as white with cloudy cores crystals and dark grey and black impurities. Yellow crystals occur, probably containing Fe-oxides. Two generations of barite are usually distinguished, which forms mineral associations with Fe, Cu, and Zn sulfides. Fine barite-I crystals form association with sulfides where pyrite is dominated. Coarse barite-II crystals have formed as a result of free growth in voids in association with sulfides dominated by marcasite. Barite-II crystals are sector-zoned and contain numerous vapour and liquid FIs. The latter tabular barite of the rectangular type was usually used for FIs investigations (Figure 7f). Coase barite crystals are characteristic of the Jan Mayen sediments, while smaller ones characterize the Loki Castle sediments.

Substitution of cations other than Ba^{2+} into barite is identified. Minor substitution of Ba^{2+} by isomorphic impurity of Sr^{2+}, followed by Ca^{2+}, and Fe^{2+} occurs in the studied vents (Table 3). Negligible substitution of Ba^{2+} by isomorphic impurity of Co^{2+} occurs only in the Loki's Castel where high whole-rock Co concentrations were determined previously [37] as simple substitutions (e.g., spin state compatibility between Co^{2+} and the divalent cation).

Table 3. EDS data of barite crystals (wt.%) collected from sediments and buoyant plume at the Troll Wall (station 5516) and Loki's Castel (stations 6147, 7049) vent fields.

Grain	Ba	Sr	Ca	Fe	Co	S	O	Total
Hydrothermally altered sediments of the Troll Wall								
1	57.60	1.99	0.26	0.44	n.d.	14.68	24.53	99.50
2	55.58	3.20	0.21	0.71	n.d.	15.14	26.53	101.37
3	57.69	1.33	n.d.*	0.51	n.d.	14.62	25.52	99.68
4	57.19	2.03	n.d.	0.93	n.d.	15.13	25.95	101.24
5	56.03	2.79	n.d.	0.60	n.d.	14.84	23.80	98.06
6	58.28	1.18	n.d.	0.57	n.d.	14.66	25.47	100.15
Mean	57.06	2.09	0.24	0.63	-	14.85	25.30	100.16
Buoyant hydrothermal plume of the Troll Wall								
7	66.78	1.70	0.40	n.d.	n.d.	14.41	16.71	100.00
8	50.10	1.41	0.49	n.d.	n.d.	13.87	30.67	96.54
9	41.49	5.32	1.30	n.d.	n.d.	15.89	35.25	99.25
Mean	52.79	2.81	0.73	-	-	14.72	27.54	98.59
Hydrothermally altered sediments of the Loki's Castel								
10	61.63	0.5	0.16	0.36	n.d.	14.66	35.85	113.16
11	60.18	n.d.	0.12	0.19	0.06	13.05	31.15	104.70
12	59.68	1.24	0.11	0.11	n.d.	13.89	35.49	110.52
13	51.31	1.22	0.05	2.16	n.d.	13.09	41.53	109.36
14	63.36	0.59	0.05	0.16	0.28	13.86	29.26	107.55
15	54.07	0.10	n.d.	0.13	0.17	12.38	35.97	102.74
16	57.76	0.94	0.10	0.29	n.d.	13.25	30.20	102.53
Mean	58.28	0.66	0.10	0.49	0.17	13.45	34.21	107.22
Buoyant hydrothermal plume of the Loki's Castel								
17	43.06	5.07	1.54	n.d.	0.04	13.37	35.88	98.95

*n.d. – not detected.

4.6. Fluid Inclusions Study

The microthermometric data were measured from two-phase FIs. The results of thermal and cryometric studies of more than 200 individual FIs in barite from hydrothermally altered sediments (Table 2, Figure 2) demonstrated that Fe, Mg and Na chlorides prevailed in the hydrothermal fluids, as evidenced by the eutectic fluid temperature from –25°C to –35°C. Ice-melting temperatures ranged from −1.7 to −2.7 °C, corresponding to salinities between 2.8 and 4.4 wt.% NaCl eq. The relatively high temperature of ice melting indicates that the fluid trapped in the FIs was diluted.

In the Troll Wall vent field, the two-phase FIs are homogenized at temperature of 115–275 °C when heated. At the same time, the salt concentration and fluid density is 2.8–4.2 wt.% eq. NaCl and 0.80–0.98 g/cm^3, respectively. In the Perle & Bruce vent field, the homogenization temperature of the two-phase FIs in barites is 159–234 °C, the salt concentration is 3.1–4.2 wt.% eq. NaCl, and the fluid density is 0.80–0.96 g/cm^3. In the Loki’s Castle vent field, the homogenization temperature of the two-phase FIs in barites is 205–287 °C, and the salt concentration is 2.8–4.4 wt% eq. NaCl and the fluid density is 0.78–0.88 g/cm^3. However, to estimate the barite crystallisation temperature through the homogenisation temperature of the FIs, a correction for the pressure corresponding to the sampling depth is necessary. Due to the different depths at the studied hydrothermal vent fields, the values of temperature pressure correction are 1–5 °C and 18–20 °C for the for the Jan Mayen and Loki’s Castle vent fields, respectively (Table 2).

Consequently, the data suggest that studied barites from the Troll Wall vent field crystallized at pressure corrected trapping temperatures at least 276 °C from a heated fluid with salinity up to 4.4 wt.% eq NaCl. The barites from the Perl & Bruce vent field crystallized at close temperature and salinity of fluid: at least 273 °C and 4.2 wt.% eq NaCl. The Loki’s Castle hydrothermal fluid reached at least 307 °C and 4.4 wt.% NaCl eq. (Figure 8). Based on the salinity of the fluid, it could have been heated ambient seawater with temperature of slightly below zero (from –0.10 °C to –0.72 °C) and salinity of 3.185 wt.% NaCl eq. The data also reveal a general dilution of hydrothermal fluid down to 2.8–3.1 wt.% NaCl eq.

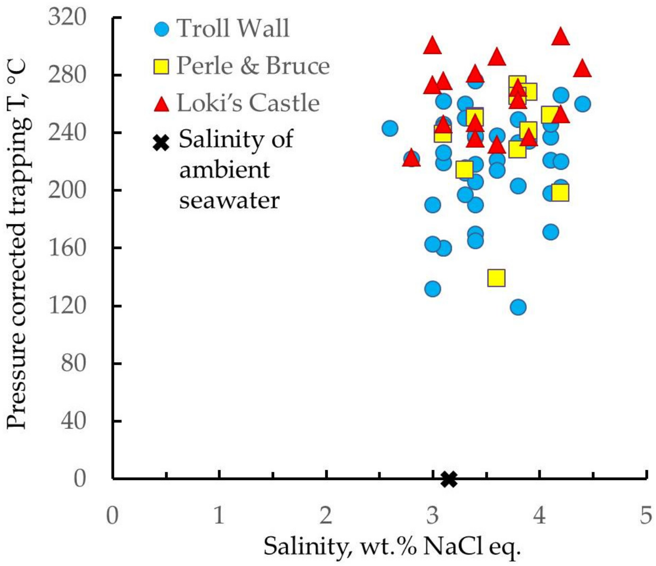

Figure 8. Fluid inclusion data hosted in barites for the Troll Wall, Perle & Bruse, and Loki’s Castle hydrothermally altered sediments. Numerical data can be found in Table 2.

5. Discussion

The studied hydrothermal systems are associated with modern submarine volcanism and located at the AVRs according to published [69] and own data. The Troll Wall hosted by S-E rift wall of the AVR what is typical for hydrothermal systems of the MAR [40]. The Perle & Bruce vent field is occupied the rift valley on the SE flank of the AVR summit what is unusual location for hydrothermal systems. The area of the vent field is exposed to detrital sediment and could be partially covered by a thin layer (2–3 cm) of pelagic clastic sediment. The sediment-influenced Loki's Castle vent field is located near the summit of the AVR. Although the active chimneys are on a basalt ridge, Baumberger et al. [33] clearly demonstrated the strong sedimentary influence into the hydrothermal circulation at Loki's Castle. The focused and diffuse venting is occurred in the studied hydrothermal fields [13,32,56]. Therefore the studied hydrothermal systems form volcanogenic massive sulfide deposits [37,40].

5.1. Hydrothermal Vent Field Settings

The ambient seawater of both sites characterized by the temperatures slightly below zero and salinity of 3.185 wt.% NaCl eq. CTD let us to reveal positive temperature anomalies with an amplitude up to 2.49 °C in the near bottom layer associated with the propagation of a neutral buoyant plume in the Jan Mayen vent field area. In the near bottom layer, water transport in a north-easterly direction was recorded, almost coinciding with the direction of the rift valley. The water movement was back-and-forth with a semidiurnal tidal cycle. Current velocities varied from 0.3 to 18.7 cm/s, averaging 6.1 cm/s [58]. The turbidity of the near-bottom layer was low.

In the area of Loki's Castle, the maximum suspended particulate matter signal was observed in the near-bottom layer up to ~250 m from seafloor. That turbidity layer does not result solely from hydrothermal activity, but instead reflects a combination of hydrothermal particles and resuspended sediments due to relatively high current velocities [32]. The area surrounding the Loki's Castle vent field site is one of the few places where substantial amounts of sediment accumulate in the mid-ocean rift valley [48].

5.2. Barite Hosted Rocks

The both vent sites are affected by neovolcanic activity [32]. Petrographic data show that samples of basalt nature occur in both hydrothermal systems, but there is a greater abundance of volcanic glasses with typical conchoidal glass fracture, hyaloclastites and basalts in the Jan Mayen vent field area than in the Loki Castle vent site. The young volcanites found in the Jan Mayen vent field area between hydrothermal sites are highly porous, which is typical of shallow volcanic outpourings [22]. The volcanic basement is covered by case sandy sediments, indicating the relative old age of the volcanic structures. The vast majority of basaltic glasses are subject to the seafloor alteration – palagonisation [38,55]. The studied glasses exhibit variable degrees of palagonitization. The volcanic glasses have vesicular structure with porphyry and microporphyry matrix dominated by split plagioclase phenocrysts and idiomorphic clinopyroxene and olivine phenocrysts. Plagioclase and smectite microliths are present in the glasses. The volcanic glasses have various alteration degrees in the Jan Mayen vent field area: from colourless, transparent and dense, to light yellow and fissured, with areas of palagonite and smectite, to a black isotropic opaque matrix composed entirely of smectite microfibres. According to the total alkalis classification [70], both whole-rock data and EDS data showed that the examined glasses belong to tachylitic and tholeiitic basalt field (see Supplementary material, Table S2).

The dark brown coarse volcanic glasses with minor alteration were found occasionally on the seafloor in the vicinity of Loki's Castle. The glassy fragments have a sparsely phyric texture, where a few microphenocrysts of plagioclase, olivine and occasional pyroxene are identified. In altered areas and along fractures, there is a fibrous ochre material, palagonite. Our data showed that the examined glasses belong to tholeiitic basalt field. In terms of petrochemical characteristics, the magmatism of the Mohns Ridge differs little from similar structures of the MAR type between latitudes of 34º and 48º N [71], i.e. the area influenced by the Azores hot spot.

5.3. Characterisation of Mineralised Material

In modern hydrothermal systems occurring in hotspots [22,24,32,72], barite is often represented in association with high-temperature minerals, which is also to be expected for the white smokes of the Jan Mayen vent fields. Barite has a lesser extent, for the black smokes of the Loki's Castle vent field. The three studied vent fields are mafic-hosted systems. The basaltic rocks of the Jan Mayen vent fields have a characteristic E-MORB signature and therefore enriched by barite in contrast to the Loki's Castle vent field with characteristic D-MORB signature [38] and barite as accompanying mineral but occasionally barite can be a gangue mineral in pyrite → gypsum → barite → goethite → talc mineral association. In Troll Wall, barite is identified as a gangue mineral in chalcopyrite → pyrite → sphalerite → barite → marcasite mineral association. The occurrence of a second generation of chalcopyrite, sphalerite and barite, and a third generation of pyrite in the association, that overprint previous generations suggesting temporal fluctuations in temperature of mineralizing fluids [73]. The crystalline precipitations of finely crystalline sphalerite on large barite crystals suggest possible high-temperature jumps of hydrothermal fluid (Figure 6e). In Perle & Bruce, barite is one of the gangue mineral in pyrite → gypsum → barite mineral association.

Thus, nonmetallic minerals predominate in the vent fields studied, and sulfide minerals are most often represented as disseminated fine grains and/or colloform textures. Complex intergrowths, replacements, and recrystallization of the minerals are reviled that resulting from a relatively dynamic and locally chaotic environment of sulfide precipitation in altered sediments [37,74]. The Jan Mayen and Loki's Castle vent fields are pyrite dominated among sulfide phases, accompanied by marcasite, sphalerite, and chalcopyrite. Other sulfide minerals are much less abundant: wurtzite only found in Troll Wall, galenite, a Pb-bearing mineral phase, is detected in both sites, and famatinite, a Cu-Sb-bearing mineral, is found in Loki's Castle. The selenium enrichment in the sediments of Loki's Castle is obviously caused by its concentration in galena, sphalerite and pyrite, i.e. relatively high-temperature sulfide minerals. The arsenic enrichment in the sediments of Perle & Bruce is caused by its co-precipitation with the hydrous ferric oxide fraction of the particles, i.e. lower-temperature mineral phase of Fe-oxides [75].

Based on EDS data of sulfide minerals from two hydrothermal mineral assemblages (barite-I → sphalerite-I → chalcopyrite-I → pyrite-II and chalcopyrite-II → pyrite-III → sphalerite-II → barite-II → marcasite-I) of the Troll Wall sediments (see Supplementary material, Table S3), the range of temperatures at which these minerals formed has been estimated previously [74]. For the pyrite–marcasite equilibrium, the S_{total} content in both minerals exceeds that for their normal chemical composition, varying from 55.1 wt.% in pyrite to 57.3 wt.% in marcasite. Applying the temperature diagram of the Fe–S system according to Predel F. [76] for a given S_{total} content, a pyrite–marcasite equilibrium formation temperature below 419 ºC was obtained, which corresponds to our data on barite crystallization temperature. At temperatures below 419 ºC, hydrothermal deposits should be dominated by sulfide assemblages with marcasite rather than pyrite, which is entirely consistent with our data. In addition, Kullerud's method, i.e. sphalerite geothermometry [77], has been applied to the studied mineral assemblages of the Troll Wall vent field. Using the FeS–ZnS equilibrium diagram by Kullerud G. [77] it was found that the decrease of isomorphic Fe impurity content from sphalerite-I to sphalerite-II corresponds to a temperature decrease from 290 ºC to 130 ºC [74].

A basic explanation of the mineralogical and geochemical diversity of deposits of the studied systems is the degree of maturity of the ore-generating hydrothermal systems, which is determined by the stages of mineral depletion of source rocks, beginning with the depletion of olivines, pyroxenes and other dark-colored minerals and finishing with feldspars [78]. The formation of the opal–barite Fe- and Zn-rich edifices of the Jan Mayen and anhydrite–talk Fe- and Cu-rich edifices of the Loki's Castle is confined to this one of the last stages of depletion. The Loki Castle may be a more mature vent field than the Jan Mayen [38]. The mineralogy of pyrrhotite-rich surface sediments of the Loki's Castle vent field suggests the first stage of alteration of seafloor sulfide sediments – halmyrolysis, according to [78], where two stages of hydrothermal sulfides halmyrolysis have been identified. Whereas pyrite- and marcasite-rich surface sediments of the Troll Wall vent field is attributed the transition between first and second stages of halmyrolysis. Finally, the mineralogy of surface sediments of the Perle & Bruce vent field exposed to the precipitation of Mn oxyhydroxides and barite suggest the second stage of halmyrolysis related to the oxidation of Fe(II). Therefore, three studied hydrothermal settings differ between each other not only by *PT*-conditions, maturity and alteration under oxic conditions but these settings demonstrate the geodiversity of hydrothermal processes inside the each system.

The barite under study, formed in association with hydrothermal activity, has the typical morphology characteristic of hydrothermal barite [1,5] and the similar shape of crystals. Barite is a good indicator of proximal hydrothermal activity. It is a typical hydrothermal product, is suggested by the high Ba content in mineralaising fluid and high SO_4^{2-} content in seawater. Barite is the predominant sulfate phase in the studied sediments of the vent fields. The predominant sulfate phase in the sediments is jarosite–gypsum–barite. Barite is the predominant sulfate phase and one of the dominated hydrothermally derived minerals in the both studied Jan Mayen vent fields, consistent with the Ba-rich hydrothermal fluids [38] penetrating into the E-MORB host rocks. Barite is therefore more common and has coarse crystals in the fields of Jan Mayen than in Loki's Castle. The predominant sulfate phase in the Loki's Castle sediments is jarosite–gypsum–barite, as well, but in dominate talc hydrothermally derived substrate of sediments, whereas according to published data [e.g., 32,37,38], in the chimney edifices talc-anhydrite-dominated substrate includes the barite–amorphous silica caps. Consequently, in the Loki's Castle deposits, barite is a subordinate mineral but its content can reach the high values corresponds for a major mineral and occasional occurrence of barite-rich mineral assemblages. That is consistent with the Ba-depleted hydrothermal fluids which can be attributed the D-MORB host rocks [38] and other *PT*-conditions in contrast to the Jan Mayen vent fields. However, the results of thermodynamic modeling by Melekestseva et al. [25] show that interaction of seawater with Ba-enriched basalt is not sufficient to produce a Ba-rich fluid and significant barite deposition on the seafloor. The evidence for fluid phase separation before barite precipitation makes this constraint even stronger. Nonetheless, the FIs study provides additional insight into the precipitation conditions of barite-rich massive sulfides in the hydrothermal systems of AMOR.

5.4. Fluid Inclusions Hosted in Barites

Our data contribute to the few studies investigating FIs hosted in anhydrite by Sahlström et al [37], where data are available, and in amorphous silica and barite by Strmic Palinkas et al [39], where data are lacking in the hydrothermal systems of the Moons Ridge. The investigated FIs were two-phase and represented a liquid-salt solution with a low-density vapour bubble. Single-phase inclusions (liquid only) are not present in the crystals studied. The presence of only one type of FIs determines the absence of FIs assemblages (coexistence of FIs of different types) in studied barites. A secondary origin of the fluid inclusions can be excluded based on morphological and textural features. No significant differences were found between FIs hosted by barite crystals from studied vent fields.

For a more correct comparison of the temperatures of studied hydrothermal fields, a box-whisker plot was used, which has previously been used to compare the physical and chemical parameters of orogenic gold deposits of different ages [28]. In the plot, the whiskers correspond to the 5th and 95th percentiles. The plot (Figure 9) shows that the higher temperature of the fluid corresponds to the Loki's Castle vent field, followed by the Perle & Bruce and finally the Troll Wall vent fields. No correlation between salinity and pressure corrected temperature of FIs has been revealed, as, for example, such a correlation was found for FIs in other minerals, such as anhydrite or amorphous silica, in other hydrothermal fields of the MAR [79]. A general cooling trend with dilution of the Fåvne hydrothermal fluid down to 4.2 wt.% NaCl eq. was previously noticed [37] as well. The absence of a temperature trend associated with changes in salinity may indicate the presence of a single main fluid source (seawater) and a lack of participation of a noticeable share of hydrothermal ore-bearing fluids in the barite mineralisation at different temperatures and it is a characteristic of volcanogenic massive sulfide deposits [27]. Earlier was already noticed [39] that FIs entrapped in barite from the Loki's Castle shows composition close to seawater, in contrast to amorphous silica hosts two-phase FI assemblages that preserve characteristics of hydrothermal ore-bearing fluids.

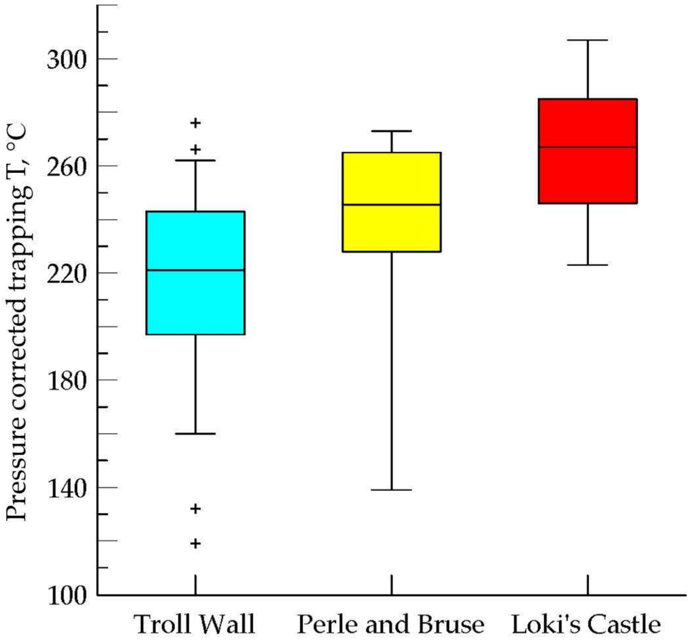

Figure 9. Comparison of trapping temperatures (pressure corrected) for fluid inclusions in barite disseminated in hydrothermally altered sediments of the studied vent fields.

5.4.1. Troll Wall Vet Field

The FIs study showed that fluids with a salinity ranging from 2.8–4.4 wt.% NaCl eq. circulated in the mineral-forming system in the Troll Wall vent field, and the pressure corrected temperatures of mineral formation is 119–276 ºC. The direct measurements [32,33] showed that the maximum temperature of the fluids discharged onto the seafloor at the Troll Wall vet field was 270 ºC. This value is close to the maximum temperature obtained by FIs study. Moreover, FIs research has shown that mineral formation at lower temperatures (119–260 ºC) also occurs in hydrothermally altered vent-field sediments. The salt content of the mid-temperature fluids emanating from the Troll Wall differs from seawater: the measured salinity ranges from 82% to 138% of seawater. But the mean value of salinity is slightly higher than seawater 3.5 ± 0.36 wt.% NaCl eq. (hear and after ±0.36 is average deviation of the data from the mean value), median value (50% quartile) is 3.4 wt.% NaCl eq. It is known [38], that the vent fluids that are discharged from the relatively shallow Jan Mayen vent fields are undergoing phase separation (boiling) at the seafloor. At this phase the fluid undergoes additional modification and is partitioned into a low-salinity, vapor-rich phase, and a metal-rich brine phase [80].

Thus, several immiscible phases and fluids of different compositions were circulating in the mineral-forming system of the Troll Wall vent field, where barite and associated Fe and Zn sulfides and Fe-Si oxyhydroxides were deposited. Our data on barite crystallization in the Troll Wall sediments is close to the temperature range obtained from sphalerite geothermometry. It is known that the homogenization temperature of FIs can differ from the crystallization temperature of the host mineral by some value, which depends primarily on the pressure [36]. If the crystallization temperature of sphalerite and barite is taken as the temperature calculated from the value of ferricity of sphalerite, then the difference between the maximum crystallization temperature and maximum homogenization temperature will be 30 ºC. This corresponds to a pressure of 430 bar (approximately 4,300 m below seafloor). Possibly we may estimate the depth of fluid–rock interaction at about 3,700 m below the seafloor.

5.4.2. Perle & Bruce Vent Field

The FIs study showed that fluids with a salinity ranging from 3.1–4.2 wt.% NaCl eq. circulated in the mineral-forming system in the Perle & Bruse vent field, and the pressure corrected temperatures of mineral formation is 139–273 ºC. The direct measurements [56,81] of emitted fluids revealed temperatures between 229 and 270 °C and lower chloride content than in seawater, indicating that the fluids had undergone phase separation. The present-day venting fluids at the Bruce vent field are less saline (about 2.6 wt.% NaCl eq.) than our data derived from FIs. Nonetheless, the salt contents derived from FIs differ from seawater: the measured salinity ranges from 97% to 132% of seawater but this difference is less significant. The mean and median values of fluid salinity (3.7 ± 0.26 wt.% NaCl eq. and 3.8 wt.% NaCl eq., respectively) are slightly higher than seawater. Moreover, there are evidences of a low-temperature (dominantly birnessite) venting at the Perle & Bruse vent field, ~2 km east of the Troll Wall vent field [21,53]. It is noteworthy that the Perle & Bruse is located not in the rift valley, but on the flank of the eastern AVR massif, at the base of the fault scarp.

5.4.3. Loki's Castel Vent Field

The FIs study showed that fluids with a salinity ranging from 2.8–4.4 wt.% NaCl eq. circulated in the mineral-forming system in the Loki's Castel vent field, and the pressure corrected temperatures of mineral formation is 223–307 ºC. The salt content of the mid-temperature fluids emanating from the Troll Wall differs from seawater: the measured salinity ranges from 88% to 138% of seawater. But the mean and median values of salinity are close to seawater 3.5 ± 0.37 wt.% NaCl eq. Previously [33], according to direct measurements from the chimney edifices, it had already been reported that the fluid salinity was less than that of seawater. Chloride concentrations different from seawater indicate that the venting fluid has undergone phase separation processes. According to [80], the Loki's Castle fluids did not phase separate at the seafloor like in the Jan Mayen vents, but phase separation occurred in or above the high-temperature reaction zone, where low density vapors rise in the hydrothermal cell and high density brines either accumulate at the base of the circulating system or rise slowly. Baumberger et al. [33] agued, that the minimum depth and temperature to produce a vapor phase with about 2.9 wt.% NaCl eq. are 650 m below the seafloor [33].

A wide variation in the crystallization temperature is typical of mineral formation in the hydrothermal vent fields of the Mohns Ridge. Our estimates of pressure corrected temperatures are consistent with the present-day temperature at the studied vents but represent the wider temperature fluctuations of mainly moderately-temperature venting of (Fe, Ba)-bearing hydrothermal fluids. The study of FIs shows that products of barite formation at lower temperatures are also found in hydrothermally altered sediments of these vents, i.e., minerals continued to crystalize also under fluid temperatures falling down to 119 ºC and 139 ºC for the Troll Wall and Perle & Bruse, respectively. The lowest temperature values may reflect the deposition of late-stage barite. The lowest temperature values obtained from the FIs are approximately 50–150 ºC lower than the present-day direct temperature measurements. Significant changes in the temperature of mineralising fluids have previously been established for a number of hydrothermal systems [79]. Moreover, measurements at 1-minute intervals with an autonomous thermometer at a black smoker of the Rainbow vent field (low-spreading MAR) showed that the temperature repeatedly fluctuated between 250 ºC and 348 ºC during 35 minutes [82]. The relatively wide pressure corrected temperature range obviously indicates the mixing of seawater and hydrothermal fluids in the highly porous massive sulfides and basalts [e.g., 83]. The fluid–rock interaction at ~2 km below the seafloor was suggested for the Loki's Castle [32] and at ~3.7 km for the Jan Mayen vents [74].

Two-phase fluids are subject to significant temperature fluctuations, which can lead to significant changes in fluid composition, primarily in salinity. The salinity of the fluids hosted in barites of the vent fields studied (at ~500–2,400 m depth) ranges from 2.6 to 4.4 wt.% NaCl eq., which is only relatively close to the salinity of the ambient seawater. A box-whisker plot was used to demonstrate the salinity variations of fluids in the studied hydrothermal systems (Figure 10). In the plot, the median (50% quartile) of salinity varied from 3.4 to 3.8 wt.% NaCl eq. and the highest value corresponds to fluids circulating in the Perle & Bruce vent field and that is slightly higher than direct measurements of the present-day venting Bruce fluids [56,81]. There is no trend between cooling the hydrothermal fluid and diluting it down to 2.6 wt.% NaCl eq. and therefore a fluid with low salinity (compared to ambient seawater) cannot simply be the result of mixing with cold seawater.

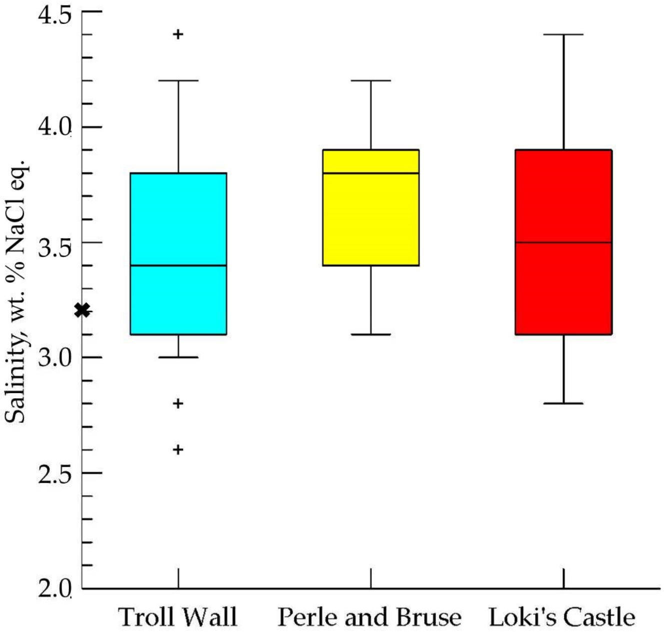

Figure 10. Comparison of salinity for fluid inclusions in barite disseminated in hydrothermally altered sediments of the studied vent fields. A cross indicates the salinity of ambient seawater.

Thus, the salt contents of hot fluids venting from the Mohns Ridge hydrothermal systems generally differ from seawater with measured salinities ranging from 82% to 138% seawater and shows much less variations than that was reported for the mid-ocean ridges ranging from 10% to 200% seawater [84]. Analysis of fluid inclusions trapped in anhydrites in the Fåvne vent field at ~3,000 m depth in the central part of the Mohns Ridge [37] showed that fluid salinities were typically about twice the salinity of the ambient seawater, but ranged from 4.2 to 8.0 wt.% NaCl eq. The reported salinity of the trapped Fåvne fluid is higher than our data derived from FIs in barites. The low-salinity fluids down to 2.6–3.1 wt.% NaCl eq. trapped in barites of studied vents could thus represent condensed vapors generated by phase separation (boiling) of a higher-salinity aqueous fluid below the seafloor [23,25]. This process produces a heavy saline brine, which mostly remains at depth, and a low-salinity vapor phase, which migrates toward the seafloor [33,80,85]. Low-salinity and low-density vapors are ascend buoyantly in the hydrothermal system, mix with cold seawater, and finally emanate at the seafloor producing low salinity (compared to seawater) vents [80]. The wide variations in fluid temperature and salinity in the studied Mohns Ridge vent fields can be explained by both temporal fluctuations, which have been verified by [33], and the circulation of several immiscible phases and fluids of different compositions in hydrothermal systems. In support of this argument, there are published data that the areas around the larger chimneys of studied fields are characterized by several locations with diffuse venting of low-temperature fluids (approximately 2–54 °C) [13,34,55,56]. The diffuse venting emanating from sediments obviously derived from the relatively high-temperature endmember fluids. Evidently, that is a common phenomenon for hydrothermal systems of the AMOR and MAR [32,40]. Except at Lucky Strike, fluids from the MAR have a single end-member composition indicating a single deep source [40].

Thus, two processes play a major role in fluid compositions: phase separation and the composition of the basement rocks [40]. High-salinity (up to 50 wt.% NaCl eq.) inclusions are thought to be of magmatic origin and low- to moderate-salinity inclusions (<1.0 and up to 15–20 wt.% NaCl eq.) have been attributed to phase separation followed by the segregation of the vapor and brine phases [80,86,87]. A comparative study with similar products from other hydrothermal vent fields is presented in Table 4 in an attempt to understand how the systems studied relate to the overall context. The salinity of the fluids differs from that of the ambient seawater, which is assumed to be the major component of the mineralising fluid in generally accepted models of submarine hydrothermal systems [79]. Venting fluids are likely to be ultimately remixed fluids that are less saline than the initially separated brine fluid as observed in the most hydrothermal systems [23,25 and references therein]. Most hydrothermal fluids have salinity variations of 2–6 times, but typically salinity is at least 5–6 times lower than that of the ambient seawater and twice as much as that of the ambient seawater. In model by Bischoff and Rosenbauer [88], mid-ocean ridges hydrothermal systems are composed of a single pass seawater cell overlying a dense, high-temperature brine cell with salinities that are at least five times seawater. The high salinity fluids are more evident from intermediate and fast spreading due to the assimilation of Cl-rich crust during crystallization in a shallow magma chamber [89]. It is believed that volcanic processes in low-spreading ridges developed above small local magmatic chambers (volcanic phase) give way to a long-lasting tectonic phase when the magmatic chamber disappears [82]. The FIs in barites of the hydrothermal systems under study show a salinity not exceeding 1.4 times that of ambient seawater. Except at the deeper Fåvne vent field [37], the salinity exceeds that of the ambient seawater by a factor of 2.3. The lowest calculated salinity of FIs in the Troll Wall is approximately 3–4 times higher than the lowest salinity of barite FIs in the Hook Ridge, Bransfield Strait (0.9 wt.% NaCl eq. [83]) and the Semenov-1 (0.6 wt.% NaCl eq. [25]), respectively, which is the lowest reported values for seafloor hydrothermal fields. Our FIs data derived from barites and published data derived from anhydrites [37] in the discussed hydrothermal vent fields of the Mohns Ridge are consistent with 90% of published homogenization temperature–salinity pairs from volcanogenic massive sulfide ore deposits summarized by Bodnar et al. [27] (Figure 11). Therefore, low- and moderate-salinity fluids circulate in the Mohns Ridge hydrothermal systems but moderate-salinity solutions relatively close to ambient seawater prevail according to FIs study in barites what is corresponds to an ultraslow-spreading ridge. Despite the temporal fluctuations in temperature and composition of mineralizing fluids revealed by Baumberger et al. [33] and proposed in our study, the hydrothermal systems of the Mohns Ridge represent a more stable chemical environment compared to those at fast-spreading ridges [90]. Such a constant emanation of hydrothermal fluids makes these hydrothermal vents on the ultraslow-spreading Mohns Ridge a relatively stable source of Ba, Fe, Zn, Cu and other trace elements to the Arctic Ocean and subpolar North Atlantic.

Table 4. Temperature of primary hydrothermal fluids at the Mid-Atlantic Ridge (MAR) and Mohns Ridge segment of the Arctic Mid-Ocean Ridge (AMOR) according to published and own data.

Vent field	Location	Depth, m	Deposit type	Fluid salinity, wt.% NaCl eq.	Fluid T*, °C	Comment	Reference
Troll Wall	71º18' N, Mohns Ridge, AMOR	550	Chimney edifices	n.d.**	260–270	Direct measurements.	[32]
		512–600	Hydrothermally altered sediments	n.d.	130–290	Sphalerite geothermometry, Kullerud's method.	[74]
		512–600	Hydrothermally altered sediments	2.6–4.4	119–276	Primary and secondary FIs in barite. Fluid phase separation indicated.	This work
Bruce	71º18' N, Mohns Ridge, AMOR	561	Barite-rich chimney edifices	~2.6	240–242	Direct measurements: maximum temperature. Fluid	[56]

						phase separation indicated.	
		560	Barite-rich chimney edifices	~2.5	229–270	Direct measurements. Fluid phase separation indicated.	[81]
Perle & Bruce	71º18' N, Mohns Ridge, AMOR	620	Hydrothermally altered sediments	3.1–4.2	139–273	Primary and primary–secondary FIs in barite. Fluid phase separation indicated.	This work
Soria Moria	71º15' N, Mohns Ridge, AMOR	~700	Chimney edifices	~3.1	50–270	Direct measurements.	[81]
Loki’s Castle	73°30' N, Mohns Ridge, AMOR	~2,000	Talc–anhydrite chimney edifices	~2.9	280–317	Direct measurements. Fluid phase separation indicated.	[33]
		2376	Hydrothermally altered sediments	2.8–4.4	223–307	Primary and secondary FIs in barite. Fluid phase separation indicated.	This work
Fåvne	72º45′ N, Mohns Ridge, AMOR	~3,000	Seafloor massive sulfide	4.2–8.0	200–291	Primary FIs in anhydrite. Fluid did not experience significant mixing with seawater.	[37]
Menez Gwen	37°50′N, MAR, influenced by the Azores hot spot	847–871	Anhydrite and Anhydrite-barite edifices with disseminated sulfides	2.2–2.3	271–284	Direct measurements. Fluid phase separation indicated.	[22]
Lucky Strike	37º N, MAR, influenced by the Azores hot spot	1618–1730	Sulfate–sulfide deposits	2.9–3.5	202–325	Direct measurements. Evidence for fluid phase separation.	[72]
Rainbow	36° 14' N and 33°54' W, MAR	2270–2320	Sulfide edifices, field associated with serpentinites	4.5–7.7	295–370	Primary FIs in anhydrite associated with marcasite and chalcopyrite. Fluid phase separation proposed.	[82]

Broken Spur	29° 10' N, 43º 10' W, MAR	~3000	Sulfide chimney, walls of a tube	3.0–6.3	259–406	Primary FIs in anhydrite. Fluid phase separation indicated.	[79]
TAG, Trans-Atlantic Geotraverse	26° 08′ N, MAR	3670	Volcanogenic massive sulfides, edifices	1.2–5.1	187–390	Primary FIs in anhydrite. Fluid phase separation indicated.	[91]
			Breccia, veins, quartz, massive granular pyrite	1.9–6.2	212–390	Primary FIs in anhydrite and quartz. Fluid phase separation indicated.	[92]
Logachev-1	14° 45' N, MAR	2970	Sulfide chimney, walls of a tube	4.2–16.2 (max 26)	271–365	Primary FIs in anhydrite. Fluid phase separation indicated.	[79]
				1.9–6.2	212–390	Primary FIs in anhydrite and quartz. Fluid phase separation indicated.	[92]
Semenov-1	13°30′ N, MAR	2,400–2,950	Barite-rich massive sulfides	0.6–3.8	83–244	Primary FIs in barite. Fluid phase separation indicated.	[25]
Ashadze 1, Long Chimney	12° 58' N, MAR	4080	Sulfide edifices	5.0–7.0	295–345	Primary FIs in anhydrite. Fluid phase separation indicated.	[93]
			Embryo sulfide edifices	5.0–7.8	235–355	Primary FIs in anhydrite. Fluid phase separation indicated.	[93]
JADE	Central Okinawa Trough, N–W Pacific. Back-arc basin.	1300–1600	Sulfide-sulfate chimneys and mounds. Stockwork mineralizations.	4.4–9.6	220–320	Primary FIs in gypsum and barite.	[94]
				2.0–15.0	270–360	Primary FIs in sphalerite. Fluid phase separation indicated.	[11]
Endeavour Segment	Juan de Fuca Ridge, N–E Pacific	2050–2700	Barite-rich sulfide edifices	5.7–9.4	124–283	Primary FIs in barite. Fluid phase separation is not confirmed.	[18]
Vienna Wood	3° 10' S, 150º 17' E, Manus basin, S–W Pacific	~2500	Barite–silica–sulfide chimney, top of an active tube	4.7–7.6	165–235	Primary and secondary FIs in barite. Fluid phase separation indicated.	[79]
				5.3–7.2	242–324	Primary FIs in anhydrite. Fluid	[79]

				4.1–8.5	160–247	phase separation indicated. Primary FIs in anhydrite associated with chalcopyrite and sphalerite. Fluid phase separation proposed.	[82]
Franklin seamount	9° 55' S, 151º 50' E, Woodlark basin, S–W Pacific	2143–2366	Barite–sulfide edifices	2.7–6.9	203–316	Primary FIs in barite. Fluid phase separation indicated.	[79]
Lau back arc basin	19º20'–22º50' S, Valu Fa Ridge, Tonga arc, S–W Pasific	1735	White Church, barite–sulfide chimneys	1.6–2.6	170–230	Primary FIs in barite. Fluid phase separation indicated.	[23]
Hook Ridge	62º 11′ S, 57º 15′ W, Bransfield Strait, Antarctica	990	Chimney and massive barite slab. Arc-shaped composite volcano	0.9–4.2	132–310	Primary FIs in barite. Fluid phase separation indicated.	[83]

* Temperatures from FIs reflect pressure-corrected homogenization temperatures, unless noted otherwise. **n.d. – not determined.

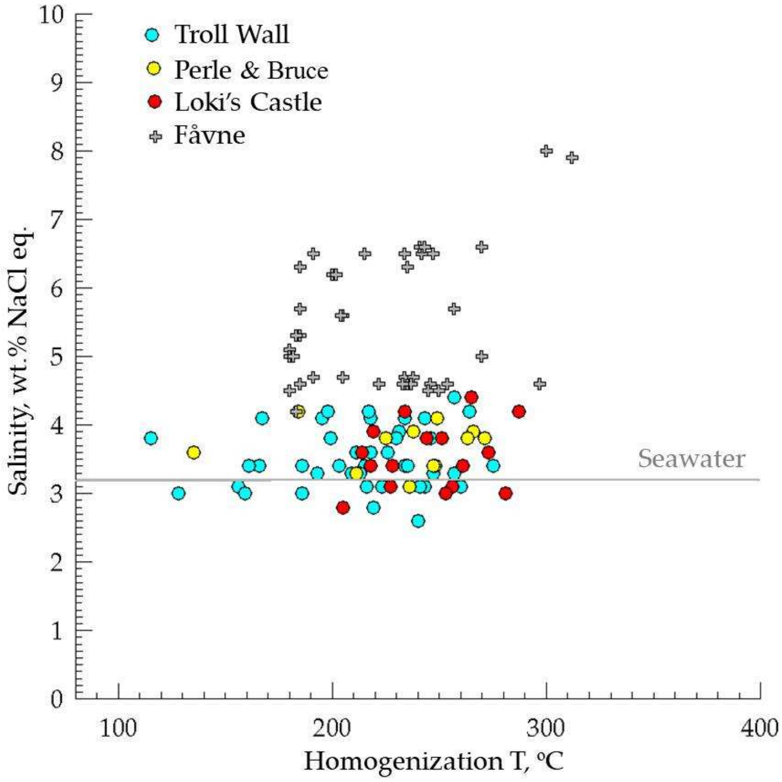

Figure 11. Trapping temperatures (pressure corrected) and corresponding salinities (wt.% NaCl eq.) for fluid inclusions in barite and anhydrite from volcanogenic massive sulfide deposits of the Mohns Ridge. Horizontal line indicates salinity of ambient seawater. Data on fluid inclusions in anhydrite from the Fåvne vent field are taken from [37]. .

6. Conclusions and Perspectives

The study of fluid inclusions hosted in barites from hydrothermally altered sediments of the Mohns Ridge represents the typical data for general fluid characteristics of the volcanogenic massive sulfide deposits [27]. Our data contribute to the few studies investigating FIs hosted in anhydrite (data are available), amorphous silica and barite (data are lacking) in the hydrothermal systems of the Moons Ridge [37,39]. The FIs from the volcanogenic massive sulfide deposits of the Mohns Ridge are mostly two-phase, liquid-plus-vapor inclusions that homogenize to the liquid phase, with salinities less than 8 wt.% NaCl eq. The studied FIs from the Jan Mayen and Loki's Castle deposits have salinities of less than 4.4 wt.% NaCl eq. and show a predominance of Fe, Mg and Na chlorides in the hydrothermal fluids. Salinity of FIs in the volcanogenic massive sulfide deposits is typically in the range 2.6–4.4 wt.% NaCl eq. or twice greater (8 wt.% NaCl eq., Fåvne vent field) than or 1.2 times less than ambient seawater salinity (3.2 wt.% NaCl eq.). The studied hydrothermal systems characterize by low- and moderate-salinity fluids and undergo fluid phase separation (boiling) below the seafloor according to generally accepted models. The phase separation produces a lower salinity phase, represented in ~24% of the FIs studied. The relatively narrow range of salinity variations measured for fluid inclusions indicate small variations in the chemistry of the hydrothermal fluids due to boiling. The revealed values of fluid salinity is corresponds to ultraslow-spreading ridges. The hydrothermal systems of the Mohns Ridge represent a more stable chemical environment compared to those at fast-spreading ridges.

Homogenization temperatures derived from barite FIs range from 115 ºC to 287 ºC in the Jan Mayen and Loki's Castle and occasionally may reach to 312 ºC derived from anhydrites FIs in the Fåvne and corresponds to the temperature (below 400 ºC) of hydrothermal convection cells that produce volcanogenic massive sulfide deposits [27]. Based on fluid inclusion data, barite precipitated from moderately-temperature (from 119 ºC to 307 ºC) sulfide–sulfate–aqueous fluids. Pressure corrected temperatures of mineralizing hydrothermal fluids vary significantly more widely than was previously suggested on the basis of direct measurements (up to 317 ºC) in the Jan Mayen and Loki's Castle. The lowest temperature values obtained from barite FIs are ~50–150 ºC lower than the present-day temperature measurements using a remotely operated underwater vehicle during cruises with the G.O. Sars research vessel. The variations in mineralising fluid temperature and salinity in the studied hydrothermal systems may reflect: (i) the deposition of late-stage barite; (ii) temporal fluctuations of ore-bearing fluids; (iii) circulation of several immiscible phases and fluids of slightly different compositions. The absence of a temperature trend related to changes in salinity is a characteristic feature of the volcanogenic massive sulfide deposits according to Bodnar et al. [27].

The data obtained emphasize the relatively stable characteristics of fluids circulating in the studied hydrothermal systems in general and slightly higher salinity of fluid in the Perle & Bruce vent field in contrast to present-day fluid measurements. In this way, this study has extended the dataset of fluid characteristics and expanded about environments of the hydrothermal systems of the Mohns Ridge. Therefore, FIs study hosted in minerals of the modern seafloor hydrothermal sites is a reliable approach not only to fill a gap in the direct measurements of hydrothermal fluids but provides more detailed knowledge of the mineralising fluids circulating in the hydrothermal system and the nature of their evolution.

Supplementary Materials: The following supporting information can be downloaded at the website of this paper posted on Preprints.org.

Author Contributions: Conceptualization, M.D.K. and A.Yu.L.; methodology, V.Yu.P. and M.D.K.; software, V.Yu.P.; validation, V.Yu.P., M.D.K. and A.Yu.L.; formal analysis, V.Yu.P., M.D.K., O.M.D., A.A.K., K.S.Ya., V.Yu.K.; investigation, M.D.K., A.A.K., B.V.B.; resources, M.D.K., V.Yu.P.; data curation, M.D.K.; writing—

original draft preparation, M.D.K.; writing—review and editing, M.D.K., V.Yu.P., B.V.B., A.Yu.L.; visualization, M.D.K., B.V.B.; supervision, M.D.K.; project administration, M.D.K.; funding acquisition, M.D.K. All authors have read and agreed to the published version of the manuscript.

Funding: This research was funded by the RUSSIAN SCIENCE FOUNDATION, grant number 20-17-00157-P, https://rscf.ru/project/20-17-00157/. Field studies were carried out within the state assignment of the Shirshov Institute of Oceanology, Russian Academy of Sciences, subject number FMWE-2021-0006.

Data Availability Statement: The original contributions presented in the study are included in the article and supplementary material, further inquiries can be directed to the corresponding author.

Conflicts of Interest: The authors declare no conflict of interest.

Acknowledgments: We acknowledge the crew and participants of the 75th cruise of the RV *Akademik Mstislav Keldysh* carried out in June 2019 for helping acquire the sediment samples. We would also like to grateful to Georgy Malafeev and Sergey Isachenko (IO RAS) for assisting with collecting the samples. We thank Andrey Boev and Alexander Filippov (IO RAS) for their assistance in analyses proceeding.

References

1. Griffith, E. M., & Paytan, A. Barite in the ocean – occurrence, geochemistry and palaeoceanographic applications. *Sedimentology* **2012**, *59*(6), 1817–1835. https://doi.org/10.1111/j.1365-3091.2012.01327.x
2. Chow, T. J., & Goldberg, E. D. On the marine geochemistry of barium. *Geochimica et Cosmochimica Acta* **1960**, *20*(3–4), 192–198. https://doi.org/10.1016/0016-7037(60)90073-9
3. Horner, T. J., Pryer, H. V., Nielsen, S. G., Crockford, P. W., Gauglitz, J. M., Wing, B. A., & Ricketts, R. D. Pelagic barite precipitation at micromolar ambient sulfate. *Nature Communications* **2017**, *8*(1). https://doi.org/10.1038/s41467-017-01229-5
4. Horner, T. J., Little, S. H., Conway, T. M., Farmer, J. R., Hertzberg, J. E., Janssen, D. J., … Wuttig, K. Bioactive Trace Metals and Their Isotopes as Paleoproductivity Proxies: An Assessment Using GEOTRACES-Era Data. *Global Biogeochemical Cycles* **2021**, John Wiley and Sons Inc. ,; https://doi.org/10.1029/2020GB006814
5. Paytan, A., Mearon, S., Cobb, K., & Kastner, M. Origin of marine barite deposits: Sr and S isotope characterization. *Geology* **2002**, *30*(8), 747–750. https://doi.org/10.1130/0091-7613(2002)030<0747:OOMBDS>2.0.CO;2
6. Lein, A. Y., & Kravchishina, M. D. Barium Geochemical Cycle in the Ocean. *Lithology and Mineral Resources* **2021**., *56*(4), 293–308. https://doi.org/10.1134/S0024490221040052
7. Martinez-Ruiz, F., Paytan, A., Gonzalez-Muñoz, M. T., Jroundi, F., Abad, M. M., Lam, P. J., … Kastner, M. Barite formation in the ocean: Origin of amorphous and crystalline precipitates. *Chemical Geology* **2019**., *511*, 441–451. https://doi.org/10.1016/j.chemgeo.2018.09.011
8. Dean, W. E., & Schreiber, B. C. Marine evaporites. S.E.P.M. Short Course 4, Oklahoma City, 1978.
9. Von Damm, K. L. Seafloor hydrothermal activity: black smoker chemistry and chimneys. *Annual Review of Earth & Planetary Sciences* **1990**, *18*, 173–204. https://doi.org/10.1146/annurev.ea.18.050190.001133
10. Tivey, M. K. Generation of seafloor hydrothermal vent fluids and associated mineral deposits. *Oceanography* **2007**, *20*(SPL.ISS. 1), 50–65. https://doi.org/10.5670/oceanog.2007.80
11. Lüders, V., Pracejus, B., & Halbach, P. Fluid inclusion and sulfur isotope studies in probable modern analogue Kuroko-type ores from the JADE hydrothermal field (Central Okinawa Trough, Japan). *Chemical Geology* **2001**, *173*(1–3), 45–58. https://doi.org/10.1016/S0009-2541(00)00267-9
12. Peters, M., Strauss, H., Petersen, S., Kummer, N. A., & Thomazo, C. Hydrothermalism in the Tyrrhenian Sea: Inorganic and microbial sulfur cycling as revealed by geochemical and multiple sulfur isotope data. *Chemical Geology* **2011**, *280*(1–2), 217–231. https://doi.org/10.1016/j.chemgeo.2010.11.011
13. Eickmann, B., Thorseth, I. H., Peters, M., Strauss, H., Bröcker, M., & Pedersen, R. B. Barite in hydrothermal environments as a recorder of subseafloor processes: A multiple-isotope study from the Loki's Castle vent field. *Geobiology* **2014**, *12*(4), 308–321. https://doi.org/10.1111/gbi.12086
14. Averyt, K. B., & Paytan, A. Empirical partition coefficients for Sr and Ca in marine barite: Implications for reconstructing seawater Sr and Ca concentrations. *Geochemistry, Geophysics, Geosystems* **2003**, *4*(5). https://doi.org/10.1029/2002GC000426
15. Albarède, F., Michard, A., Minster, J. F., & Michard, G. ^{87}Sr^{86}Sr ratios in hydrothermal waters and deposits from the East Pacific Rise at 21°N. *Earth and Planetary Science Letters* **1981**, *55*(2), 229–236. https://doi.org/10.1016/0012-821X(81)90102-3

16. Monnin, C., Jeandel, C., Cattaldo, T., & Dehairs, F. The marine barite saturation state of the world's oceans. *Marine Chemistry* **1999**, *65*(3–4), 253–261. https://doi.org/10.1016/S0304-4203(99)00016-X
17. Hannington, M. D., Jonasson, I. R., Herzig, P. M., & Petersen, S. Physical and chemical processes of seafloor mineralization at mid-ocean ridges. In *Geophysical Monograph Series* **1995**, *91*, pp. 115–157). Blackwell Publishing Ltd. https://doi.org/10.1029/GM091p0115
18. Jamieson, J. W., Hannington, M. D., Tivey, M. K., Hansteen, T., Williamson, N. M. B., Stewart, M., … Langer, J. Precipitation and growth of barite within hydrothermal vent deposits from the Endeavour Segment, Juan de Fuca Ridge. *Geochimica et Cosmochimica Acta* **2016**, *173*, 64–85. https://doi.org/10.1016/j.gca.2015.10.021
19. Lein, A. Y., Bogdanov, Y. A., & Lisitzin, A. P. Processes of hydrothermal ore genesis in the World Ocean: The results of 35 years of research. *Doklady Earth Sciences* **2016**, *466*(1), 38–41. https://doi.org/10.1134/S1028334X16010050
20. Hsieh, Y. T., Bridgestock, L., Scheuermann, P. P., Seyfried, W. E., & Henderson, G. M. Barium isotopes in mid-ocean ridge hydrothermal vent fluids: A source of isotopically heavy Ba to the ocean. *Geochimica et Cosmochimica Acta* **2021**, *292*, 348–363. https://doi.org/10.1016/j.gca.2020.09.037
21. Bogdanov, Y. A., Lisitzin, A. P., Binns, R. A., Gorshkov, A. I., Gurvich, E. G., Dritz, V. A., … Kuptsov, V. M. Low-temperature hydrothermal deposits of Franklin Seamount, Woodlark Basin, Papua New Guinea. *Marine Geology* **1997**, *142*(1–4), 99–117. https://doi.org/10.1016/S0025-3227(97)00043-1
22. Bogdanov, Y. A., Lein, A. Y., & Sagalevich, A. M. Chemical composition of the hydrothermal deposits of the Menez Gwen vent field (Mid-Atlantic Ridge). *Oceanology* **2005**, *45*(6), 849–856.
23. Lécuyer, C., Dubois, M., Marignac, C., Gruau, G., Fouquet, Y., Ramboz, C. Phase separation and fluid mixing in subseafloor back arc hydrothermal systems; a microthermometric and oxygen isotope study of fluid inclusions in the barite–sulfide chimneys of the Lau Basin. *Journal of Geophysical Research* **1999**, *104*, 911–928.
24. Lein, A. Y., Bogdanov, Y. A., Maslennikov, V. V., Li, S., Ulyanova, N. V., Maslennikova, S. P., & Ulyanov, A. A. Sulfide minerals in the Menez Gwen nonmetallic hydrothermal field (Mid-Atlantic Ridge). *Lithology and Mineral Resources* **2010**, *45*(4), 305–323. https://doi.org/10.1134/S0024490210040012
25. Melekestseva, I. Y., Tret'yakov, G. A., Nimis, P., Yuminov, A. M., Maslennikov, V. V., Maslennikova, S. P., … Large, R. Barite-rich massive sulfides from the Semenov-1 hydrothermal field (Mid-Atlantic Ridge, 13°30.87′ N): Evidence for phase separation and magmatic input. *Marine Geology* **2014**, *349*, 37–54. https://doi.org/10.1016/j.margeo.2013.12.013
26. Bodnar R.J., Vityk M.O. Interpretation of microthermometric data for H_2O–NaCl fluid inclusions. In *Fluid inclusions in minerals: methods and applications*. Pontignano: Siena, 1994; pp. 117–130.
27. Bodnar, R. J., Lecumberri-Sanchez, P., Moncada, D., & Steele-MacInnis, M. Fluid Inclusions in Hydrothermal Ore Deposits. In *Treatise on Geochemistry: Second Edition,* Elsevier Inc., 2014, Volume 13; pp. 119–142. https://doi.org/10.1016/B978-0-08-095975-7.01105-0
28. Prokofiev V.Yu., Naumov V.B. Physicochemical Parameters and Geochemical Features of Ore-Forming Fluids for Orogenic Gold Deposits Throughout Geological Time. *Minerals* **2020**, *10 (1).* 50.
29. Prokofiev, V.Y.; Naumov, V.B. Ranges of Physical Parameters and Geochemical Features of Mineralizing Fluids at Porphyry Deposits of Various Types of the Cu-Mo-Au System: Evidence from Fluid Inclusions Data. *Minerals* **2022**, *12, (5),* 529.
30. Elsgaard, L., Isaksen, M. F., Jørgensen, B. B., Alayse, A. M., & Jannasch, H. W. Microbial sulfate reduction in deep-sea sediments at the Guaymas Basin hydrothermal vent area: Influence of temperature and substrates. *Geochimica et Cosmochimica Acta* **1994**, *58*(16), 3335–3343. https://doi.org/10.1016/0016-7037(94)90089-2_
31. Chi, G., Diamond, L. W., Lu, H., Lai, J., & Chu, H. Common problems and pitfalls in fluid inclusion study: A review and discussion. *Minerals* **2021**. https://doi.org/10.3390/min11010007
32. Pedersen, R. B., Rapp, H. T., Thorseth, I. H., Lilley, M. D., Barriga, F. J. A. S., Baumberger, T., … Jorgensen, S. L. Discovery of a black smoker vent field and vent fauna at the Arctic Mid-Ocean Ridge. *Nature Communications* **2010**, *1*(8). https://doi.org/10.1038/ncomms1124
33. Baumberger, T., Früh-Green, G. L., Thorseth, I. H., Lilley, M. D., Hamelin, C., Bernasconi, S. M., … Pedersen, R. B. Fluid composition of the sediment-influenced Loki's Castle vent field at the ultra-slow spreading Arctic Mid-Ocean Ridge. *Geochimica et Cosmochimica Acta* **2016**, *187*, 156–178. https://doi.org/10.1016/j.gca.2016.05.017

34. Stensland, A., Baumberger, T., Mork, K. A., Lilley, M. D., Thorseth, I. H., & Pedersen, R. B. ^{3}He along the ultraslow spreading AMOR in the Norwegian-Greenland Seas. *Deep-Sea Research Part I: Oceanographic Research Papers* **2019**, *147*, 1–11. https://doi.org/10.1016/j.dsr.2019.04.004
35. Roedder E. Fluid inclusions: Reviews in Mineralogy 1984, Volume 12, 646 p.
36. Naumov, V. B., Dorofeeva, V. A., & Mironova, O. F. (2009). Principal physicochemical parameters of natural mineral-forming fluids. *Geochemistry International*, *47*(8), 777–802. https://doi.org/10.1134/S0016702909080035
37. Sahlström, F., Strmić Palinkaš, S., Hjorth Dundas, S., Sendula, E., Cheng, Y., Wold, M., & Pedersen, R. B. (2023). Mineralogical distribution and genetic aspects of cobalt at the active Fåvne and Loki's Castle seafloor massive sulfide deposits, Arctic Mid-Ocean Ridges. *Ore Geology Reviews*, *153*. https://doi.org/10.1016/j.oregeorev.2022.105261
38. Cruz M.I.F.S. Mineralogy and Geochemistry of contrasting hydrothermal systems on the Arctic Mid Ocean Ridge (AMOR): The Jan Mayen and Loki's Castle vent fields. Doutoramento em Ciências do Mar. Univeridadae de Lisboa. Faculdade de Ciências. 2015. 257 p.
39. Strmic Palinkas, S., Pedersen, R. B., & Sahlström, F. (2020). Sulfide Mineralization and Fluid Inclusion Characteristics of Active Ultramafic- and Basalt-Hosted Hydrothermal Vents Located along the Arctic Mid-Ocean Ridges (AMOR) (pp. 2472–2472). Geochemical Society. https://doi.org/10.46427/gold2020.2472
40. Fouquet, Y., Cambon, P., Etoubleau, J., Charlou, J. L., Ondréas, H., Barriga, F. J. A. S., … Rouxel, O. Geodiversity of hydrothermal processes along the Mid-Atlantic Ridge and ultramafic-hosted mineralization: A new type of oceanic Cu-Zn-Co-Au volcanogenic massive sulfide deposit. *Geophysical Monograph Series* **2013**, *188*, 321–367. https://doi.org/10.1029/2008GM000746
41. Klingelhöfer, F., Géli, L., Matias, L., Steinsland, N., & Mohr, J. Crustal structure of a super-slow spreading centre: A seismic refraction study of Mohns Ridge, 72°N. *Geophysical Journal International* **2000**, *141*(2), 509–526. https://doi.org/10.1046/j.1365-246X.2000.00098.x
42. Juliani, C., & Ellefmo, S. L. Probabilistic estimates of permissive areas for undiscovered seafloor massive sulfide deposits on an Arctic Mid-Ocean Ridge. *Ore Geology Reviews* **2018**, *95*, 917–930. https://doi.org/10.1016/j.oregeorev.2018.04.003
43. Geli, L., Renard, V., & Rommevaux, C. Ocean crust formation processes at very slow spreading centers: a model for the Mohns Ridge, near 72°N, based on magnetic, gravity, and seismic data. *Journal of Geophysical Research* **1994**, *99*(B2), 2995–3013. https://doi.org/10.1029/93JB02966
44. Kokhan A.V., Dubinin E.P., Grokhol'sky A.L. Geodynamic features of the structure generation in the spreading ridges of Arctic and Polar Atlantic // Vestnik KRAUNTS. Earth Sciences. 2012. №1. Vol.19. P. 59-77 (in Russian)
45. Reimers, H. The Morphology of the Mohn's Ridge with Special Focus on Listric and Detachment Faults and their Link to the Formation of Seafloor-massive Sulfides. Thesis Norwegian University of Science and Technology, Department of Geoscience and Petroleum, 2017. https://ntnuopen.ntnu.no/ntnu-xmlui/bitstream/handle/11250/2452116/14120_FULLTEXT.pdf?sequence=1
46. Pedersen, R. B., Thorseth, I. H., Nygård, T. E., Lilley, M. D., & Kelley, D. S. Hydrothermal Activity at the Arctic Mid-Ocean Ridges. In *Diversity of Hydrothermal Systems on Slow Spreading Ocean Ridges*, Wiley, 2013; pp. 67–89. https://doi.org/10.1029/2008GM000783
47. Schander, C., Rapp, H. T., Kongsrud, J. A., Bakken, T., Berge, J., Cochrane, S., … Pedersen, R. B. (2010). The fauna of hydrothermal vents on the Mohn Ridge (North Atlantic). *Marine Biology Research*, *6*(2), 155–171. https://doi.org/10.1080/17451000903147450_
48. Johannessen, K. C., Vander Roost, J., Dahle, H., Dundas, S. H., Pedersen, R. B., & Thorseth, I. H. Environmental controls on biomineralization and Fe-mound formation in a low-temperature hydrothermal system at the Jan Mayen Vent Fields. *Geochimica et Cosmochimica Acta* **2017**, *202*, 101–123. https://doi.org/10.1016/j.gca.2016.12.016
49. Snook, B., Drivenes, K., Rollinson, G. K., & Aasly, K. Characterisation of mineralised material from the Loki's castle hydrothermal vent on the Mohn's ridge. *Minerals* **2018**, *8*(12). https://doi.org/10.3390/min8120576
50. Ramirez-Llodra E, Hilario A, Paulsen E, Costa CV, Bakken T, Johnsen G and Rapp HT. Benthic Communities on the Mohn's Treasure Mound: Implications for Management of Seabed Mining in the Arctic Mid-Ocean Ridge. Front. Mar. Sci. **2020**, 7:490. doi: 10.3389/fmars.2020.00490

51. Elkins, L. J., Hamelin, C., Blichert-Toft, J., Scott, S. R., Sims, K. W. W., Yeo, I. A., … Pedersen, R. B. North Atlantic hotspot-ridge interaction near Jan Mayen Island. *Geochemical Perspectives Letters* **2016**, *2*(1), 55–67. https://doi.org/10.7185/geochemlet.1606
52. Pedersen, RB, Bjerkgård, T. Sea-floor massive sulphides in Arctic waters. In: *Mineral Resources in the Arctic*. 2016; pp 209–216. Retrieved from https://www.ngu.no/upload/Aktuelt/CircumArtic/5_SMS.pdf
53. Kravchishina, M. D., Kuznetsov, A. B., Baranov, B. V., Dara, O. M., Starodymova, D. P., Klyuvitkin, A. A., … Lein, A. Y. Hydrothermal Genesis of Fe–Mn Crust in the Southernmost Segment of the Mohns Ridge, Norwegian Sea: REE Geochemistry and Sr and Nd Isotopic Composition. *Doklady Earth Sciences* **2022**, *506*(2), 734–739. https://doi.org/10.1134/S1028334X22600530
54. Klyuvitkin, A. A., Kravchishina, M. D., Nemirovskaya, I. A., Baranov, B. V., Kochenkova, A. I., & Lisitzin, A. P. Studies of Sediment Systems of the European Arctic during Cruise 75 of the R/V Akademik Mstislav Keldysh. *Oceanology* **2020**, *60*(3), 421–423. https://doi.org/10.1134/S0001437020030030
55. Kruber, C., Thorseth, I. H., & Pedersen, R. B. Seafloor alteration of basaltic glass: Textures, geochemistry, and endolithic microorganisms. *Geochemistry, Geophysics, Geosystems* **2008**, *9*(12). https://doi.org/10.1029/2008GC002119
56. Stokke, R., Reeves, E. P., Dahle, H., Fedøy, A. E., Viflot, T., Lie Onstad, S., … Steen, I. H. Tailoring Hydrothermal Vent Biodiversity Toward Improved Biodiscovery Using a Novel in situ Enrichment Strategy. *Frontiers in Microbiology* **2020**, *11*. https://doi.org/10.3389/fmicb.2020.00249
57. Humphris, S. E., Tivey, M. K., & Tivey, M. A. The Trans-Atlantic Geotraverse hydrothermal field: A hydrothermal system on an active detachment fault. *Deep-Sea Research Part II: Topical Studies in Oceanography* **2015**, *121*, 8–16. https://doi.org/10.1016/j.dsr2.2015.02.015
58. Klyuvitkin, A. A., Kravchishina, M. D., & Boev, A. G. Particle Fluxes in Hydrothermal Vent Fields of the Southern Part of the Mohns Ridge. *Doklady Earth Sciences* **2021**, *497*(1), 200–205. https://doi.org/10.1134/S1028334X21030053
59. Kravchishina, M. D., Novigatskii, A. N., Savvichev, A. S., Pautova, L. A., & Lisitsyn, A. P. (2019). Studies on Sedimentary Systems in the Barents Sea and Norwegian–Greenland Basin during Cruise 68 of the R/V Akademik Mstislav Keldysh. *Oceanology*, *59*(1), 158–160. https://doi.org/10.1134/S0001437019010053
60. **Bezrukov,** P.L., **Lisitzin,** A.P. Classification of bottom sediments in modern marine reservoirs. *Trudy Inst. Oceanol.* **1960,** 32, 3–14. (In Russian)
61. Lisitzin, A.P. Oceanic Sedimentation: Lithology and Geochemistry. American Geophysical Union, Washington, D. C. 1996. https://doi.org/10.1002/9781118665008
62. Brown P.E. & Lamb W M. *P-V-T* properties of fluids in the system H_2O ± CO_2 ± NaCl: New graphical presentations and implications for fluid inclusion studies // Geochimica et Cosmochimica Acta. 1989. V.53. № 6. P. 1209-1222.
63. Borisenko A. S. Cryometric study of salt composition of gas–liquid inclusions in minerals. *Russian Geol. and Geofis.* 1977, *No.8*, 16–27.
64. Brown P. FLINCOR: a computer program for the reduction and investigation of fluid inclusion data // Amer. Mineralogist. 1989. V. 74. P. 1390–1393.
65. Turekian et al. Geological Society of America Bulletin Distribution of the Elements in Some Major Units of the Earth ' s Crust. *Geological Society of America BulletinAmerica* **1961**, *72*, 175–192.
66. Boström, K., Peterson, M. N. A., Joensuu, O., & Fisher, D. E. Aluminum-poor ferromanganoan sediments on active oceanic ridges. *Journal of Geophysical Research* **1969**, *74*(12), 3261–3270. https://doi.org/10.1029/JB074i012p03261
67. Bonatti, E., & Joensuu, O. Deep-sea iron deposit from the South Pacific. *Science* **1966**, *154*(3749), 643–645. https://doi.org/10.1126/science.154.3749.643
68. Bonatti E. Kraemer T., Rydell H. Classification and genesis of submarine iron-manganese deposits, 1972.
69. Stubseid, H.H., Bjerga, A., Haflidason, H., Pedersen, R. B. Volcanic evolution of an ultraslow-spreading ridge. *Nature Portfolio* **2023**, Preprint. DOI: 10.21203/rs.3.rs-2393567/v1
70. Bas, M. J. L., Maitre, R. W. L., Streckeisen, A., & Zanettin, B. A chemical classification of volcanic rocks based on the total alkali-silica diagram. *Journal of Petrology* **1986**, *27*(3), 745–750. https://doi.org/10.1093/petrology/27.3.745
71. Sushchevskaya, N. M., G. A. Cherkashev, T. I. Tsekhonya, Yu. A. Bogdanov, B. V. Belyatskiy, and N. N. Kononkova Magmatism of Mon and Knipovich ridges, polar Atlantics spreading zones, petrogeochemical

study, Mid-Atlantic Ridge. *Russian Journal of Earth Sciences* **2000**, *2*(3–4), 243–267. https://doi.org/10.2205/2000ES000043

72. Langmuir C., Humphris S., D. Fomari, C. Van Dover, K. Von Damm, M.K. Tivey, D. Colodner, J.-L. Charlou D. Desonie, I C. Wilson, Y. Fouquet, G. Klinkhammer, H. BougaultHydrothermal vents near a mantle hot spot: the Lucky Strike vent field at 370 N on the Mid-Atlantic Ridge. *Earth and Planetary Science Letters* **1997**, *48*, 69–91.
73. Eldridge, C. S., Barton, P. B., & Ohmoto, H. Mineral Textures and Their Bearing on Formation of the Kuroko Orebodies. In *The Kuroko and Related Volcanogenic Massive Sulfide Deposits*. Society of Economic Geologists, 2019. https://doi.org/10.5382/mono.05.15
74. Kravchishina, M. D., Lein, A. Y., Boev, A. G., Prokofiev, V. Y., Starodymova, D. P., Dara, O. M., … Lisitzin, A. P. Hydrothermal Mineral Assemblages at 71° N of the Mid-Atlantic Ridge (First Results). *Oceanology* **2019**, *59*(6), 941–959. https://doi.org/10.1134/S0001437019060109
75. Feely, R. A., Gendron, J. F., Baker, E. T., & Lebon, G. T. Hydrothermal plumes along the East Pacific Rise, 8°40′ to 11°50′N: Particle distribution and composition. *Earth and Planetary Science Letters* **1994**, *128*(1–2), 19–36. https://doi.org/10.1016/0012-821X(94)90023-X
76. Phase Equilibria, Crystallographic and Thermodynamic Data of Binary Alloys. Phase Equilibria, Crystallographic and Thermodynamic Data of Binary Alloys. Springer Berlin Heidelberg, 2016. https://doi.org/10.1007/978-3-642-24977-8
77. Kullerud G. The FeS–ZnS system, a geological thermometer // Norsk Geologisk Tiddsskrift. 1953. V. 32. P. 61–147.
78. Maslennikov, V. V., Cherkashov, G. A., Firstova, A. V., Ayupova, N. R., Beltenev, V. E., Melekestseva, I. Y., … Blinov, I. A. Trace Element Assemblages of Pseudomorphic Iron Oxyhydroxides of the Pobeda-1 Hydrothermal Field, 17°08.7′ N, Mid-Atlantic Ridge: The Development of a Halmyrolysis Model from LA-ICP-MS Data. *Minerals* **2023**, *13*(1). https://doi.org/10.3390/min13010004
79. Bortnikov, N. S., Simonov, V. A., & Bogdanov, Y. A. Fluid inclusions in minerals from modern sulfide edifices: Physicochemical conditions of formation and evolution of fluids. *Geology of Ore Deposits* **2004**, *46*(1), 64–75.
80. Fontaine, F. J., & Wilcock, W. S. D. Dynamics and storage of Brine in mid-ocean ridge hydrothermal systems. *Journal of Geophysical Research: Solid Earth* **2006**, *111*(6). https://doi.org/10.1029/2005JB003866
81. Dahle, H., Le Moine Bauer, S., Baumberger, T., Stokke, R., Pedersen, R. B., Thorseth, I. H., & Steen, I. H. Energy landscapes in hydrothermal chimneys shape distributions of primary producers. *Frontiers in Microbiology* **2018**, *9*(JUL). https://doi.org/10.3389/fmicb.2018.01570
82. Bogdanov, Y. A., Bortnikov, N. S., Vikent'ev, I. V., Lein, A. Y., Gurvich, E. G., Sagalevich, A. M., … Apollonov, V. N. Mineralogical-geochemical peculiarities of hydrothermal sulfide ores and fluids in the rainbow field associated with serpentinites, Mid-Atlantic Ridge (36°C14′ N). *Geologiya Rudnykh Mestorozhdenij* **2002**, *44*(6), 510–543.
83. Petersen, S., Herzig, P. M., Schwarz-Schampera, U., Hannington, M. D., & Jonasson, I. R. Hydrothermal precipitates associated with bimodal volcanism in the Central Bransfield Strait, Antarctica. *Mineralium Deposita* **2004**, *39*(3), 358–379. https://doi.org/10.1007/s00126-004-0414-3
84. Von Damm, K. L. Controls on the chemistry and temporal variability of seafloor hydrothermal fluids. In *Geophysical Monograph Series*, **1995**, Volume 91, Blackwell Publishing Ltd.; pp. 222–247. https://doi.org/10.1029/GM091p0222
85. Von Damm, K. L. Systematics of and postulated controls on submarine hydrothermal solution chemistry. *Journal of Geophysical Research* **1988**, *93*(B5), 4551–4561. https://doi.org/10.1029/JB093iB05p04551
86. Kelley, D. S., Gillis, K. M., & Thompson, G. Fluid evolution in submarine magma-hydrothermal systems at the Mid- Atlantic Ridge. *Journal of Geophysical Research* **1993**, *98*(B11). https://doi.org/10.1029/93jb01432
87. Kelley, D.S., Shank, T.M. Hydrothermal systems: a decade of discovery in slow spreading environments. In: Rona, P.A., et al. (Eds.), "Diversity of Hydrothermal Systems on Slow Spreading Ocean Ridges" Geophysical monograph, 188, , 2010; pp. 369–407.
88. Bischoff, J. L., & Rosenbauer, R. J. Salinity variations in submarine hydrothermal systems by layered double-diffusive convection. *Journal of Geology* **1989**, *97*(5), 613–623. https://doi.org/10.1086/629338
89. Michael, P. J., & Cornell, W. C. Influence of spreading rate and magma supply on crystallization and assimilation beneath mid-ocean ridges: Evidence from chlorine and major element chemistry of mid-ocean

ridge basalts. *Journal of Geophysical Research: Solid Earth* **1998**, *103*(8), 18325–18356. https://doi.org/10.1029/98jb00791

90. Koschinsky, A., Schmidt, K., & Garbe-Schönberg, D. Geochemical time series of hydrothermal fluids from the slow-spreading Mid-Atlantic Ridge: Implications of medium-term stability. *Chemical Geology* **2020**, *552*. https://doi.org/10.1016/j.chemgeo.2020.119760
91. Tivey, M. K., Mills, R. A., & Teagle, D. A. H. Temperature and salinity of fluid inclusions in anhydrite as indicators of seawater entrainment and heating in the TAG active mound. *Proceedings of the Ocean Drilling Program: Scientific Results* **1998**, *158*, 179–190. https://doi.org/10.2973/odp.proc.sr.158.211.1998
92. Petersen, S., Herzig, P. M., & Hannington, M. D. Fluid inclusion studies as a guide to the temperature regime within the TAG hydrothermal mound, 26°N, Mid-Atlantic Ridge. *Proceedings of the Ocean Drilling Program: Scientific Results* **1998**, *158*, 163–178. https://doi.org/10.2973/odp.proc.sr.158.210.1998
93. Bortnikov, N. S., Simonov, V. A., Fouquet, Y., & Amplieva, E. E. Phase separation of fluid in the Ashadze deep-sea modern submarine hydrothermal field (mid-atlantic ridge, 12°58s′ N): Results of fluid inclusion study and direct observations. *Doklady Earth Sciences* **2010**, *435*(1), 1446–1449. https://doi.org/10.1134/S1028334X10110085
94. The appendix contain the data supplemental to the main text for this article The appendix contain the data supplemental to the main text for this article Hou, Z., & Zhang, Q. CO_2-Hydrocarbon fluids of the Jade hydrothermal field in the Okinawa trough: Fluid inclusion evidence. *Science in China, Series D: Earth Sciences* **1998**, *41*(4), 408–415. https://doi.org/10.1007/BF02932693